NEUROSCIENCE

Mate discrimination among subspecies through a conserved olfactory pathway

Mohammed A. Khallaf[1], Thomas O. Auer[2], Veit Grabe[1], Ana Depetris-Chauvin[1], Byrappa Ammagarahalli[3]*, Dan-Dan Zhang[4], Sofía Lavista-Llanos[1], Filip Kaftan[5], Jerrit Weißflog[5], Luciano M. Matzkin[6], Stephanie M. Rollmann[3], Christer Löfstedt[4], Aleš Svatoš[5], Hany K. M. Dweck[1†], Silke Sachse[1], Richard Benton[2], Bill S. Hansson[1‡§], Markus Knaden[1‡§]

Communication mechanisms underlying the sexual isolation of species are poorly understood. Using four subspecies of *Drosophila mojavensis* as a model, we identify two behaviorally active, male-specific pheromones. One functions as a conserved male antiaphrodisiac in all subspecies and acts via gustation. The second induces female receptivity via olfaction exclusively in the two subspecies that produce it. Genetic analysis of the cognate receptor for the olfactory pheromone indicates an important role for this sensory pathway in promoting sexual isolation of subspecies, in combination with auditory signals. Unexpectedly, the peripheral sensory pathway detecting this pheromone is conserved molecularly, physiologically, and anatomically across subspecies. These observations imply that subspecies-specific behaviors arise from differential interpretation of the same peripheral cue, reminiscent of sexually conserved detection but dimorphic interpretation of male pheromones in *Drosophila melanogaster*. Our results reveal that, during incipient speciation, pheromone production, detection, and interpretation do not necessarily evolve in a coordinated manner.

INTRODUCTION

One of the central questions in evolutionary biology is how populations within a species split to form new species. Divergence in sexual communication—male traits and female preferences (*1*)—has been proposed as one of the substantial forces that results in reproductive isolation. This divergence is more pronounced in allopatric populations as a by-product of ecological adaptation to different environments (*2*). However, despite numerous documented interspecific sexual traits and preferences in animals, the genetic and neural correlates of their evolution remain elusive (*3*).

Sexual traits of drosophilid flies differ quantitatively and qualitatively between species and act as premating isolation barriers (*4*). Such traits therefore represent attractive models to determine the genetic basis of phenotypic evolution. Flies identify con-subspecific mating partners through integration of different sensory modalities such as vision, audition, olfaction, and gustation, which promote courtship of appropriate mates and inhibit courtship of inappropriate partners. Insights have been gained regarding the evolution of different sensory modalities that relate to the interspecific variations in male traits or female perception among drosophilids [e.g., vision (*5*), audition (*6*), and taste (*7*, *8*)]. However, although many studies have reported the diversity of volatile pheromones in drosophilid males (*9*), the evolution of the corresponding neural changes remains little studied.

In *Drosophila melanogaster*, sex pheromones are detected by chemosensory receptors [e.g., odorant receptors (ORs)] (*10*) expressed in sensory neurons housed in hair-like structures called sensilla. Volatile pheromone-responsive ORs represent an ideal set of candidate genes to address the evolutionary basis of various sexual traits in drosophilid flies for several reasons. First, pheromone ORs are expected to be the fastest evolving chemosensory receptors, with new receptors emerging either by sequence variation or gene loss/duplication (*11*), to match the marked diversity of pheromones among closely related species (*9*). Second, the neural processing of some drosophilid pheromones [e.g., (*Z*)-11-octadecenyl acetate—*cis*-vaccenyl acetate (*c*VA)—in *D. melanogaster*] in the brain is well understood (*10*). Third, pheromone ORs are narrowly tuned to fly odors and govern robust and distinct behaviors via labeled-line circuitry (*12*–*15*). Fourth, olfactory sensory neurons (OSNs) that express pheromone ORs target sexually dimorphic pheromone-processing units (i.e., antennal lobe glomeruli) (*12*). Last, of 52 OSN classes in *D. melanogaster* (*16*), only four pheromone OR–expressing OSNs are localized in one particular class of sensilla [Or67d neuron in antennal trichoid 1 (at1) and Or47b, Or65a/b/c, and Or88a neurons in at4] (*17*). This small number compared with other non–pheromone-detecting OSNs (*17*) makes a comprehensive evolutionary study feasible.

One remarkable drosophilid is *Drosophila mojavensis*, which represents a model of incipient speciation and host adaptation (*18*). This species has four geographically isolated and ecologically distinct populations (*19*) [taxonomically classified as subspecies (*20*)] that diverged ~0.25 million years ago (Fig. 1A) (*18*, *19*). The northern subspecies *Drosophila moj. wrigleyi* and *Drosophila moj. mojavensis* use prickly pear cacti in Santa Catalina Island and red barrel cactus in the Mojave Desert, respectively, as host fruit. The southern subspecies *Drosophila moj. sonorensis* and *Drosophila moj. baja* breed and feed on the organ pipe cactus in the mainland Sonoran Desert

[1]Department of Evolutionary Neuroethology, Max Planck Institute for Chemical Ecology, Hans-Knöll-Straße 8, D-07745 Jena, Germany. [2]Center for Integrative Genomics, Faculty of Biology and Medicine, University of Lausanne, CH-1015 Lausanne, Switzerland. [3]Department of Biological Sciences, University of Cincinnati, Cincinnati, OH 45221, USA. [4]Department of Biology, Lund University, SE-22362 Lund, Sweden. [5]Group of Mass Spectrometry and Proteomics, Max Planck Institute for Chemical Ecology, Hans-Knöll-Straße 8, D-07745 Jena, Germany. [6]Department of Entomology, University of Arizona, 1140 E. South Campus Drive, Tucson, AZ 85721, USA.
*Present address: Faculty of Forestry and Wood Sciences, Czech University of Life Sciences, 165 00 Prague, Czech Republic.
†Present address: Department of Molecular, Cellular, and Developmental Biology, Yale University, New Haven, CT 06520, USA.
‡These authors share senior authorship.
§Corresponding author. Email: mknaden@ice.mpg.de (M.K.); hansson@ice.mpg.de (B.S.H.)

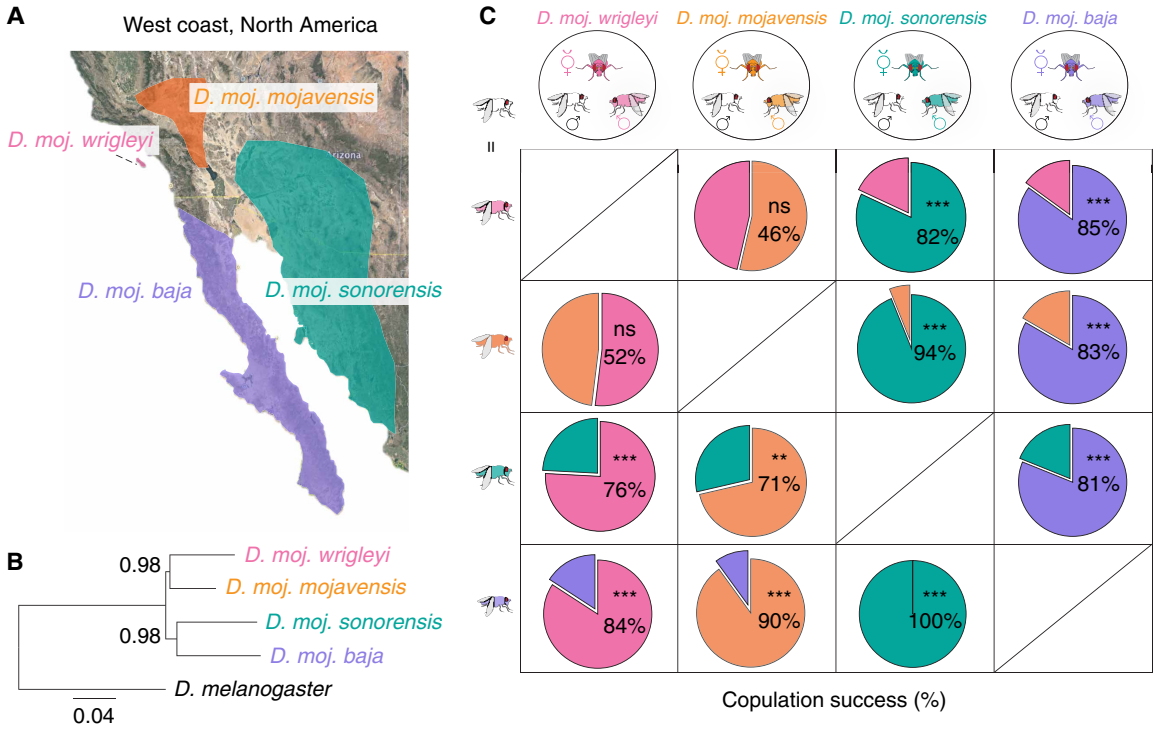

Fig. 1. Sexual isolation among *D. mojavensis* subspecies. (**A**) Geographic distribution of *D. mojavensis* subspecies on the west coast of North America. Pink, *D. moj. wrigleyi*; orange, *D. moj. mojavensis*; turquoise, *D. moj. sonorensis*; violet, *D. moj. Baja*. Adapted with permission from (*20*). (**B**) Phylogenetic relationship of *D. mojavensis* subspecies based on concatenated sequences of 9087 genes available from (*22*) (see fig. S1A and Materials and Methods for details). Scale bar for branch length represents the number of substitutions per site. Bootstrap values are indicated by the numbers at the nodes. (**C**) Top row: Competition mating arenas where a female of each *D. mojavensis* subspecies had the choice to mate with a con-subspecific male or a male of one of the other three subspecies [color coded as in (A)]. Below: Pie charts represent the percentages of copulation success of the rival males. ns, $P > 0.05$; $^{**}P < 0.01$; $^{***}P < 0.001$, χ^2 test (n from left column to right column = 84, 84, 76, 52, 84, 80, 88, 68, 92, 80, 72, and 64 replicates). See fig. S1 (B to H) for details regarding the differences and similarities of sexual behaviors among the four subspecies, and fig. S1I for details on the courtship preference indices of males between con-subspecific and hetero-subspecific females.

and the agria cactus in Baja California, respectively (*21*). Phylogenetic analyses revealed that the two northern subspecies and the two southern subspecies cluster with each other (Fig. 1B and fig. S1A) (*22*). These closely related subspecies exhibit many differences in their morphology (*20*), neurophysiological responses (*23*), genomic and transcriptomic characteristics (*18*, *22*), and behavioral traits (*24*). Experimental reciprocal crosses between these allopatric subspecies resulted in viable fertile offspring, indicating the presence of prezygotic isolation mechanisms (*25*, *26*). Previous evidence suggested that cuticular hydrocarbons contribute to this isolation barrier (*27*), but no specific chemicals have been isolated. Here, we identify these pheromones and elucidate the evolution of the underlying sensory mechanisms across subspecies to reveal the neurogenetic basis of incipient speciation.

RESULTS

Sexual isolation among incipient subspecies of *D. mojavensis*

We compared the courtship ritual among the four subspecies of *D. mojavensis* by recording the sexual behaviors of con-subspecific couples in a single-pair courtship arena (movies S1 to S4). *D. mojavensis* subspecies displayed comparable courtship rituals including a trait not described in other drosophilids—dropping behavior—in which males release a liquid droplet from their anus while licking the female's genitalia (fig. S1, B to H).

We asked whether *D. mojavensis* flies can distinguish con-subspecific and hetero-subspecific partners. As copulation success is influenced by both male courtship intensity and female receptivity (*4*), we first examined whether males exhibit courtship preference toward con-subspecific females. To distinguish male sexual behaviors from female acceptance, males were offered the choice to court either a freeze-killed con-subspecific or hetero-subspecific female (fig. S1I). Males exhibited equal preferences between females, regardless of their subspecies (fig. S1I).

Next, we investigated whether females of the different subspecies are able to distinguish their con-subspecific males by offering a female of each subspecies the choice to mate with a con-subspecific male or a male of one of the other three subspecies (Fig. 1C). Competition experiments with the two northern subspecies revealed that females did not distinguish con-subspecific and hetero-subspecific males (Fig. 1C). By contrast, southern females strongly preferred to copulate with their con-subspecific males (Fig. 1C). Both northern and southern females efficiently discriminated northern and southern males (Fig. 1C). These results suggest that while a complete sexual isolation barrier has been established both between the northern and southern subspecies, and between the southern subspecies, the northern subspecies are not yet completely sexually isolated.

D. mojavensis subspecies have distinct, but overlapping, profiles of candidate pheromones

To identify candidate pheromones that could mediate the observed sexual isolation barriers between subspecies, we analyzed the chemical profiles of males, virgin females, and mated females of several independent isolates of each subspecies. We discovered four previously unknown male-specific acetates (Fig. 2, A and B and fig. S2A) as (*R*) and (*S*) enantiomers of (*Z*)-10-heptadecen-2-yl acetate (R&S-HDEA), heptadec-2-yl acetate (HDA), and (*Z*,*Z*)-19,22-octacosadien-1-yl acetate (OCDA). Males of all four subspecies carried OCDA, while only males of the northern subspecies produced HDEA (both *R* and *S* enantiomers in similar ratio [fig. S2, B and C)] and HDA (Fig. 2, A and B, and fig. S2, A and A′). The chemical profiles of the virgin females were similar among the different subspecies (Fig. 2A and fig. S2A), which might explain the males' inability to distinguish between them (fig. S1I). However, mated females carried male-specific compound(s), indicating that these are transferred from males to females during mating (Fig. 2, A and B, and fig. S2A). Using matrix-assisted laser desorption/ionization–time-of-flight (MALDI-TOF) analyses to directly visualize pheromones on the fly body (see Materials and Methods for details), we confirmed the existence of OCDA on the male and mated female cuticle, but not on the virgin females (fig. S2, D and E).

We next investigated whether production of the male-specific compounds correlates with male sexual maturity and copulation performance. Males of the four subspecies did not exhibit any copulation during the first 5 days after eclosion (i.e., in the absence of the acetates), showed low copulation success rates at the age of 6 days (when low amounts of acetates were already detected), and successfully mated from the seventh day onward (Fig. 2C). These observations suggest that the identified male-specific acetates define the sexual maturity status of males.

The ubiquitous pheromone, OCDA, acts as conserved male antiaphrodisiac via contact chemosensation

We asked whether transfer of any male-specific compounds contributes to a general postcopulation mate-guarding strategy in *D. mojavensis* [as described for transferred pheromones in *D. melanogaster* (*28*, *29*)]. The identical chemical profiles of the two northern subspecies and of the two southern subspecies led us to focus our attention on one representative for each group. Males of *D. moj. wrigleyi* and *D. moj. sonorensis* spent more time courting virgin than mated con-subspecific females (Fig. 3A). To test which, if any, of the identified compounds contribute to courtship reduction, we perfumed virgin con-subspecific females with one of the four male-specific compounds [consistency of perfuming and correspondence to biologically relevant amounts were confirmed by gas chromatography–mass spectrometry (GC-MS) analysis; see Materials and Methods]. Only OCDA treatment of females led to a significantly reduced male courtship index (Fig. 3B and fig. S3A).

To investigate how males detect OCDA, we first tested the volatility of male-specific acetates (including OCDA) by collecting headspace samples of *D. moj. wrigleyi* males (fig. S3B). This revealed that only R&S-HDEA and HDA are volatile (fig. S3B), indicating that the nonvolatile OCDA is likely to be detected by gustation. During courtship, neural inputs from foreleg gustatory sensilla are used to evaluate the potential mating partner (*4*). We therefore investigated whether male foreleg tarsi detect OCDA (Fig. 3C). OCDA, but not the other acetates, elicited a response in a subset of tarsal sensilla (class 5b) of both *D. mojavensis* subspecies (Fig. 3C and fig. S3, C and D). Consistent with these sensilla mediating detection of OCDA, males lacking their tarsi spend equal time courting the hexane-perfumed and OCDA-perfumed females (Fig. 3D). We propose that OCDA has a conserved role across the *D. mojavensis* subspecies as a contact chemosensory signal that suppresses male courtship of mated females.

R-HDEA promotes subspecies-specific female sexual receptivity through olfaction

To examine the functions of the other previously unknown male-specific acetates in female sexual behaviors, we scored the copulation success and latency for *D. moj. wrigleyi* and *D. moj. sonorensis* females courted by con-subspecific males. Males were perfumed with one of the four male-specific acetates or hexane. Copulation success and courtship indices did not differ between the acetate- and hexane-perfumed males in both subspecies (Fig. 4A and figs. S3E and S4A). However, females of *D. moj. wrigleyi* were significantly quicker to accept the R-HDEA–perfumed males but not the males perfumed with the other acetates (Fig. 4B and fig. S4B). We extended this analysis by performing competition assays, in which a virgin female of each subspecies was allowed to choose between two con-subspecific males perfumed with hexane or with one of the four acetates. Only R-HDEA–perfumed males exhibited copulation advantage over the controls in *D. moj. wrigleyi* and *D. moj. mojavensis*, while *D. moj. sonorensis* and *D. moj. baja* females had comparable preferences between the two males (Fig. 4C and fig. S4, C and D). These results indicate that R-HDEA increases sexual receptivity in females of northern but not southern subspecies.

As R-HDEA is volatile (fig. S3B), we screened for OSNs that detect R-HDEA in *D. moj. wrigleyi* via single sensillum recordings (SSR). We identified a single antennal trichoid sensillum class, at4 (based on presumed homology to the *D. melanogaster* at4 sensillum; see below), that responds strongly to R-HDEA and HDA (Fig. 4, D and E, and fig. S4, E to G). Our extensive screening of *D. moj. sonorensis* OSNs, as well as limited recordings in *D. moj. mojavensis* and *D. moj. baja*, revealed a presence of a sensillum with identical response properties in all four subspecies (Fig. 4, E and F, and fig. S4, E and H). Together, R-HDEA activates homologous olfactory channels in all subspecies of *D. mojavensis* and enhances sexual receptivity in *D. moj. wrigleyi* but not in *D. moj. sonorensis* females.

Conserved peripheral sensory pathways for R-HDEA detection

To define the genetic basis of R-HDEA detection in *D. mojavensis* subspecies, we focused on a subset of receptors, which was previously shown to be expressed in trichoid OSNs and to detect pheromones in *D. melanogaster* (*12*, *13*, *17*, *30*). Five orthologous genes are present in the *D. moj. wrigleyi* genome (*11*): *Or47b1*, *Or47b2*, *Or65a*, *Or67d*, and *Or88a* (fig. S5A). We first visualized their expression in the antenna of *D. moj. wrigleyi* and *D. moj. sonorensis* by RNA in situ hybridization and detected expression of all receptors with a slightly increased number of *Or65a*- and *Or67d*-expressing cells in *D. moj. wrigleyi* (Fig. 5, A and B). We then asked which of these ORs is responsible for R-HDEA detection by functional expression in *Xenopus laevis* oocytes (Fig. 5C). We could detect significant depolarization upon R-HDEA application for OR47b1 and OR65a (Fig. 5D and fig. S5B). To validate these results, we generated transgenic flies expressing *D. moj. wrigleyi* ORs individually in vivo in the at1 "decoder" neuron

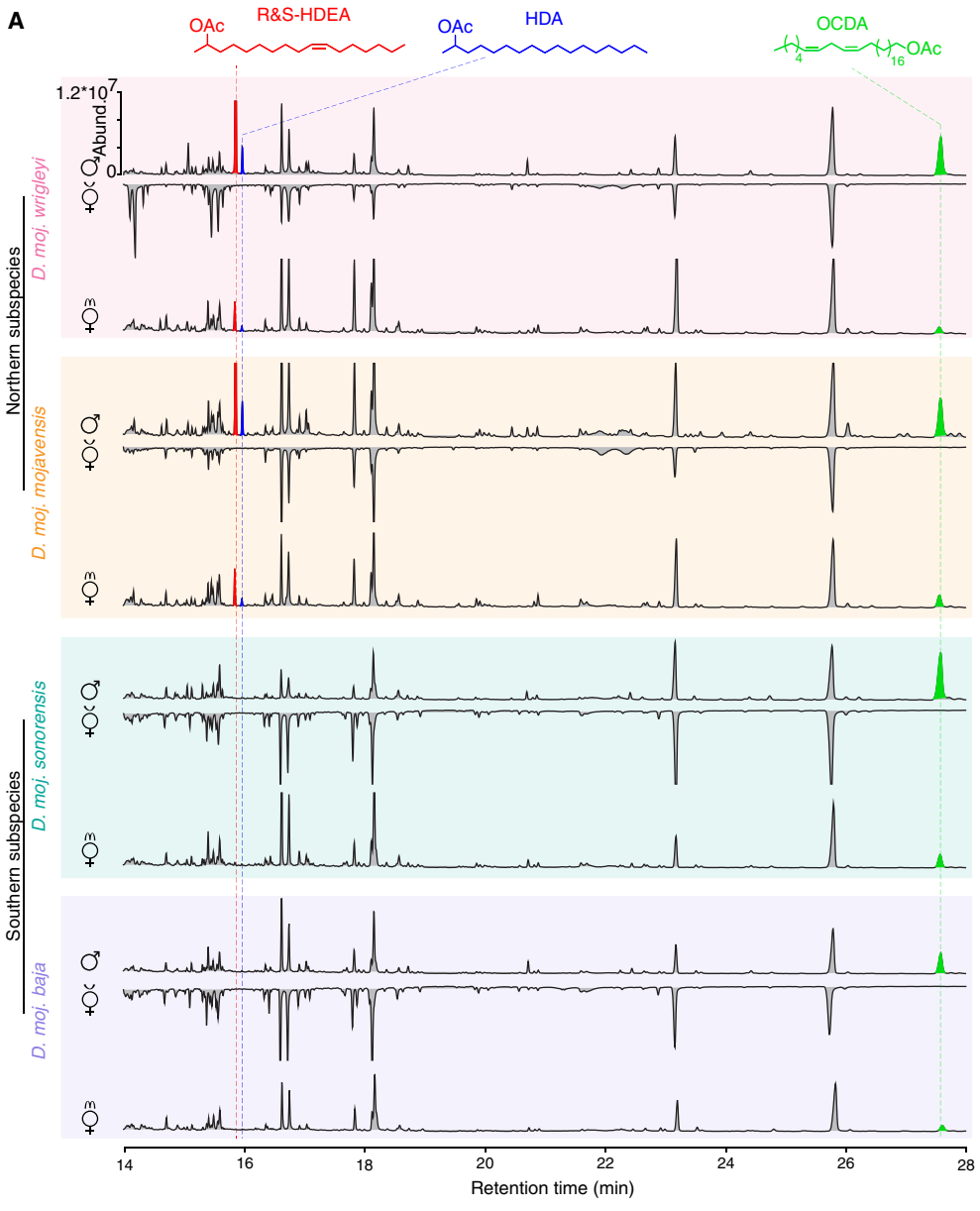

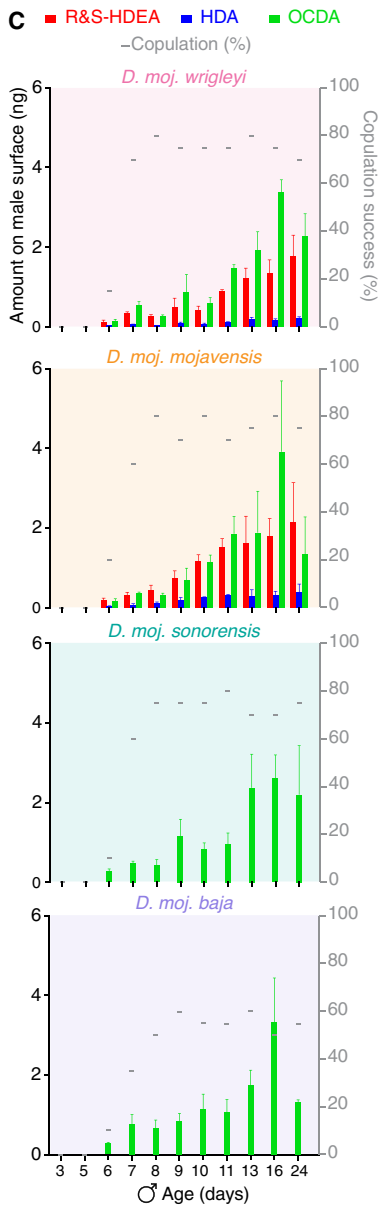

B

Male-transferred compounds	*D. moj. wrigleyi*	*D. moj. mojavensis*	*D. moj. sonorensis*	*D. moj. baja*
R/S-HDEA and HDA	+	+	–	–
OCDA	+	+	+	+

Fig. 2. Distinct, but overlapping, male-specific compounds of *D. mojavensis* subspecies. (**A**) Representative gas chromatograms of 10-day-old male (virgin, ♂) and female flies (virgin, v♀; mated, m♀) ($n = 7$) obtained by solvent-free thermal desorption–gas chromatography–mass spectrometry (TD-GC-MS) (*13*). Colored peaks indicate the male-specific compounds (see Materials and Methods for chemical syntheses), which are transferred to females during mating. Red, *R* and *S* enantiomers of (*Z*)-10-heptadecen-2-yl acetate (R&S-HDEA); blue, heptadec-2-yl acetate (HDA); and light green, (*Z*,*Z*)-19,22-octacosadien-1-yl acetate (OCDA). Different colored backgrounds represent the different subspecies (similar to Fig. 1A). Unless otherwise noted, in this and other panels, *D. moj. wrigleyi* (15081-1352.22), *D. moj. mojavensis* (15081-1352.47), *D. moj. sonorensis* (15081-1351.01), and *D. moj. Baja* (15081-1351.04) were used. Two more strains of each subspecies (see table S1 for details) were analyzed showing very similar profiles (fig. S2A′). See fig. S2A for details regarding the body wash extracts analyzed by body washes. (**B**) Summary table of the different male-transferred compounds of all *D. mojavensis* subspecies. (**C**) Amount of the male-specific compounds and corresponding copulation performance. Colored bars and error bars indicate mean amounts and SEM of the three male-specific acetates ($n = 3$ males per age); gray dashes indicate the percentage of copulation success for males of the same age within a 10-min time window ($n = 20$ males per age). See fig. S2F for the production site of these male-specific compounds.

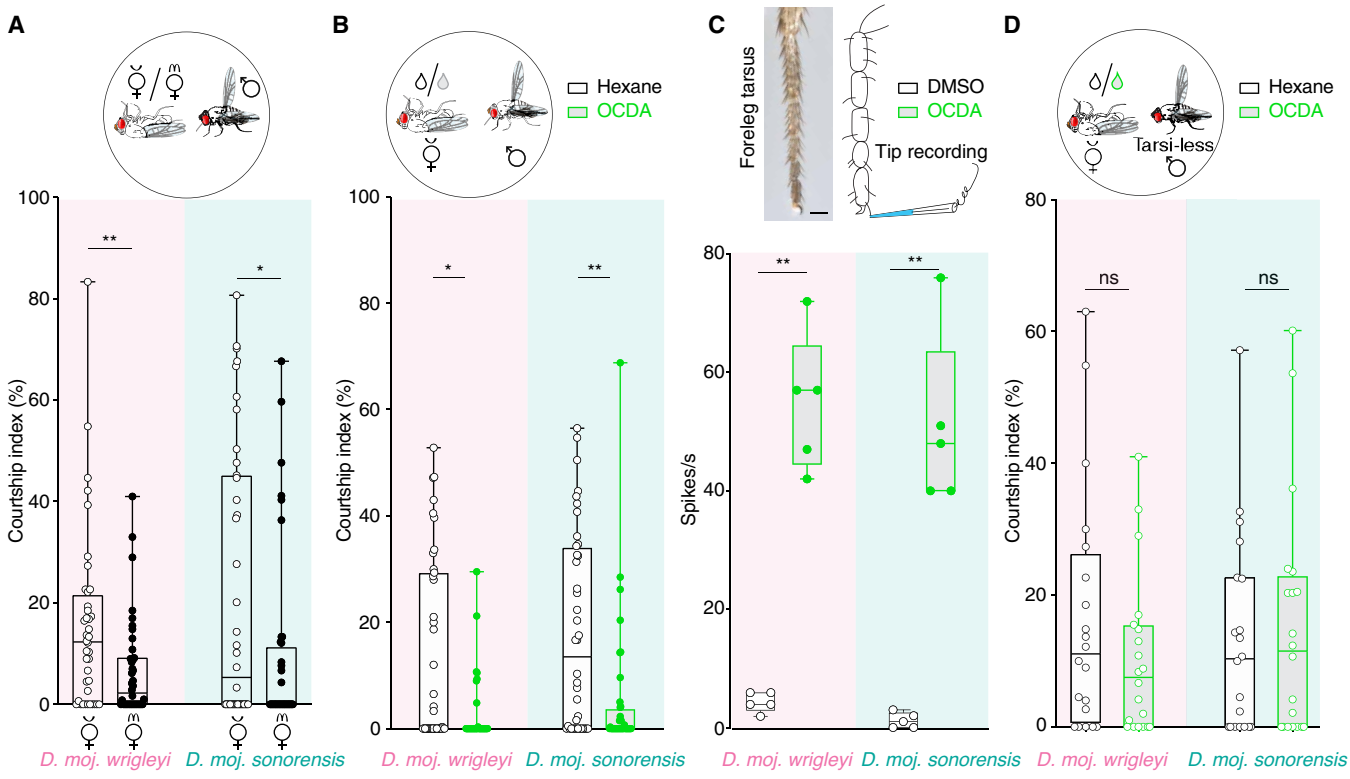

Fig. 3. Conserved behavioral responses among *D. mojavensis* subspecies to OCDA. (**A**) Top: Schematic of courtship arena where a dead (virgin or mated) female (*D. moj. wrigleyi* and *D. moj. sonorensis*) was presented to a con-subspecific male. Below: *y* axis represents courtship index (%) [equal the time a male exhibits courtship behaviors (fig. S1B)/total amount of recording time (10 min)]. In this and other panels, filled circles indicate significant difference between the tested groups; $^{*}P < 0.05$; $^{**}P < 0.01$; Mann Whitney *U* test ($n = 40$). Males and females used in this and other panels are 10 days old. (**B**) Top: Schematic of a male courting a dead virgin female of the same subspecies perfumed with hexane as a control (black) or OCDA diluted in hexane (light green). Below: Kruskal-Wallis test between different treatments in fig. S3A with Dunn's post hoc correction. ns, $P > 0.05$; $^{*}P < 0.05$; $^{**}P < 0.01$ ($n = 40$ assays). See fig. S3A for the role of the other male-specific acetates in male courtship suppression in both subspecies. (**C**) Left top: Micrograph of tarsal segments of the foreleg showing different sensory hairs. Scale bar, 50 μm (Photo credit: V.G., Max Planck Institute for Chemical Ecology). Right top: Schematics of tip recordings from the foreleg tarsal sensillum (class 5b). Below: Tip recording measurements from foreleg-tarsi of *D. moj. wrigleyi* and *D. moj. sonorensis* males using DMSO or OCDA. Kruskal-Wallis test between different treatments in fig. S3D with Dunn's post hoc correction. ns, $P > 0.05$; $^{**}P < 0.01$ ($n = 5$). See fig. S3C for tip recording traces and fig. S3D for electrophysiological responses to the other male-specific acetates. (**D**) Top: Schematic of a tarsiless male courting a dead virgin conspecific female. Below: Courtship indices of tarsiless males tested with a dead virgin female of the same subspecies perfumed with hexane (black) or OCDA (light green). ns, $P > 0.05$, Mann Whitney *U* test ($n = 20$ assays).

of *D. melanogaster* that lacks its endogenous receptor OR67d (Fig. 5E) (*12*). SSR analysis of these flies revealed that OR65a, but not OR47b1, is the sole detector for R-HDEA and HDA (Fig. 5F and fig. S5C). As predicted by the similar responses of at4 sensilla to R-HDEA and OR65a sequence similarity between both subspecies (Fig. 4, E and G, and fig. S5G), transgenic expression of *D. moj. sonorensis* OR65a in the decoder neuron revealed comparable responses to R-HDEA (Fig. 5G).

To determine whether *Or65a* is required for the enhanced female receptivity in *D. moj. wrigleyi*, we generated a loss-of-function allele of this gene using CRISPR-Cas9 genome editing (Fig. 5H and fig. S5, E and F). *Or65a* mutant females completely lack responses to R-HDEA (Fig. 5I), display no preference for R-HDEA–perfumed males (Fig. 5J and fig. S5D), and take longer to initiate copulation (Fig. 5J'). These findings confirm that OR65a is responsible for the increased female receptivity in *D. moj. wrigleyi* toward con-subspecific males.

We next analyzed the targeting pattern of Or65a OSNs to glomeruli in the antennal lobe. Comparative morphological analyses revealed a high similarity in the basic architecture of this olfactory center in *D. moj. wrigleyi* and *D. moj. sonorensis* (Fig. 5K and movies S5 and S6), but with apparently at least three additional glomeruli compared with the well-characterized antennal lobe of *D. melanogaster* (fig. S6A). Previous genetic tracing of at4 OSNs in *D. melanogaster* revealed projections to three glomeruli: Or47b neurons to VA1v, Or88a neurons to VA1d, and Or65a/b/c neurons to DL3 (*17*). To label these neurons in *D. mojavensis* subspecies, in the absence of binary effector systems, we backfilled at4 sensillum neurons with a fluorescent dye. In both *D. moj. wrigleyi* and *D. moj. sonorensis*, we detected projections to three glomeruli: VA1v, VA1d, and a glomerulus not present in *D. melanogaster* that we named "VA8" (Fig. 5L, fig. S6B, and movies S7 and S8; for terminology, see Materials and Methods). Given the conserved innervation patterns of OSNs in the *D. melanogaster* clade (*8*, *31*, *32*), it is likely that VA1v and VA1d are innervated by Or47b and Or88a neurons in *D. mojavensis*, as in *D. melanogaster*. If this assumption is correct, then our observations imply that Or65a neurons target the VA8 glomerulus in *D. mojavensis*—contrasting with the DL3 innervation pattern in *D. melanogaster*—although future development of genetic reporters in *D. mojavensis* will be necessary to confirm this proposition.

Pheromone-responsive glomeruli often display sex-specific volume differences (*33*). Volumetric analysis of the glomeruli innervated by at 4 neurons in both subspecies revealed that *D. moj. wrigleyi* VA8 is

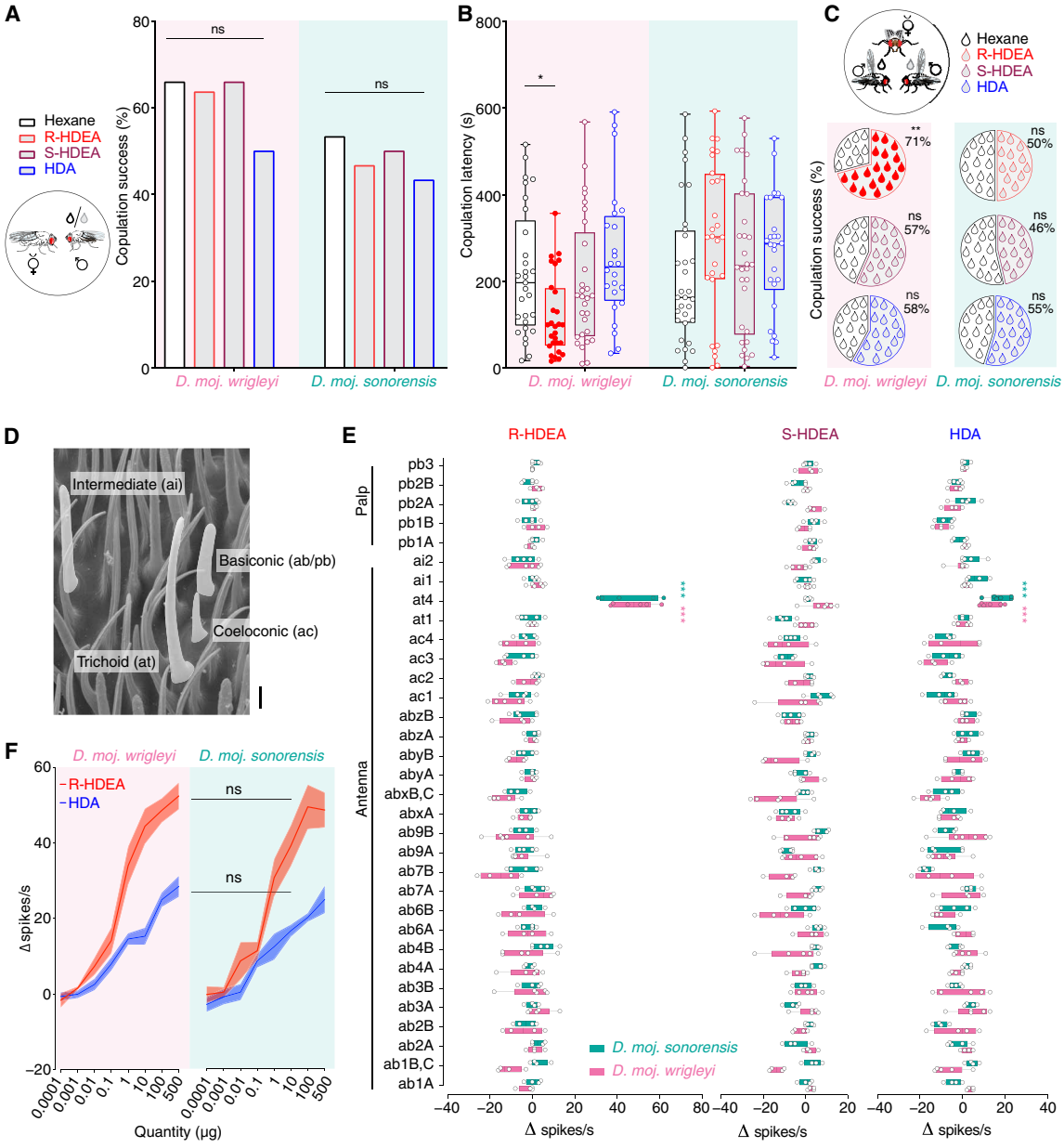

Fig. 4. R-HDEA provokes divergent sexual behaviors through activation of homologous sensory neurons. (**A**) Left: Schematic of mating arena where a perfumed male courts a virgin con-subspecific female. Black droplet, hexane (control); gray droplet, one of the other three male-transferred compounds. Right: Copulation success of *D. moj. wrigleyi* and *D. moj. sonorensis* males perfumed with hexane or male-specific acetates. Fisher's exact test. ns, $P > 0.05$ ($n = 40$ assays per treatment). See fig. S4A for OCDA impact on copulation success and fig. S3E for courtship indices of hexane- and acetates-perfumed males toward females of the same subspecies. (**B**) Copulation latencies of the same males as in (A). Filled circles indicate significant differences from the solvent. Kruskal-Wallis test with Dunn's post hoc correction. ns, $P > 0.05$; $^{*}P < 0.05$ [n from left to right represent successful copulations in (A) = 29, 28, 29, 24, 32, 28, 30, and 26 assays]. See fig. S4B for OCDA impact on females' copulation latencies. (**C**) Competition between two con-subspecific males, perfumed with one of the three compounds (colored droplet) or with the solvent hexane (black droplet), to copulate with a virgin female of the same subspecies. Pie charts represent copulation success of the rival males. Filled droplets indicate significant difference between the tested groups. χ^2 test; ns, $P > 0.05$; $^{**}P < 0.01$; from top to bottom = 124, 120, 124, 104, 112, and 116 assays. See fig. S4C for the competition results of OCDA-perfumed males and fig. S4D for *D. moj. mojavensis* and *D. moj. Baja* competition experiments. (**D**) Scanning electron micrograph of antennal surface, showing different sensillum types (intermediate, trichoid, coeloconic, and basiconic). Scale bar, 2 μm (Photo credit: V.G., Max Planck Institute for Chemical Ecology). (**E**) Electrophysiological responses toward R-HDEA, S-HDEA, and HDA in all types of olfactory sensilla on antenna and maxillary palp of *D. moj. wrigleyi* (pink) and *D. moj. sonorensis* (turquoise). Mann Whitney *U* test; ns, $P > 0.05$; $^{***}P < 0.001$ ($n = 3$ to 6 neurons). ab, antennal basiconic; ac, antennal coeloconic; at, antennal trichoid; ai, antennal intermediate; pb, palp basiconic. See fig. S4 (E to H) for similarity between male and female responses to R-HDEA, OCDA responses, representative SSR traces, and responses of R-HDEA among *D. mojavensis* subspecies, respectively. (**F**) Dose-dependent responses of at4 neurons in *D. moj. wrigleyi* and *D. moj. sonorensis* toward R-HDEA (in red) and HDA (in blue) (mean ± SEM). Two-way analysis of variance (ANOVA) followed by Sidak's multiple comparison test between the two subspecies' responses to the same stimulus; ns, $P > 0.05$ ($n = 4$ to 6 neurons). See fig. S4I for *D. melanogaster* at1 and at4 responses to *D. moj. wrigleyi*–specific acetates and fig. S4J for alignments of *D. moj. wrigleyi*–OR65a and *D. melanogaster*–OR65a/b/c protein sequences.

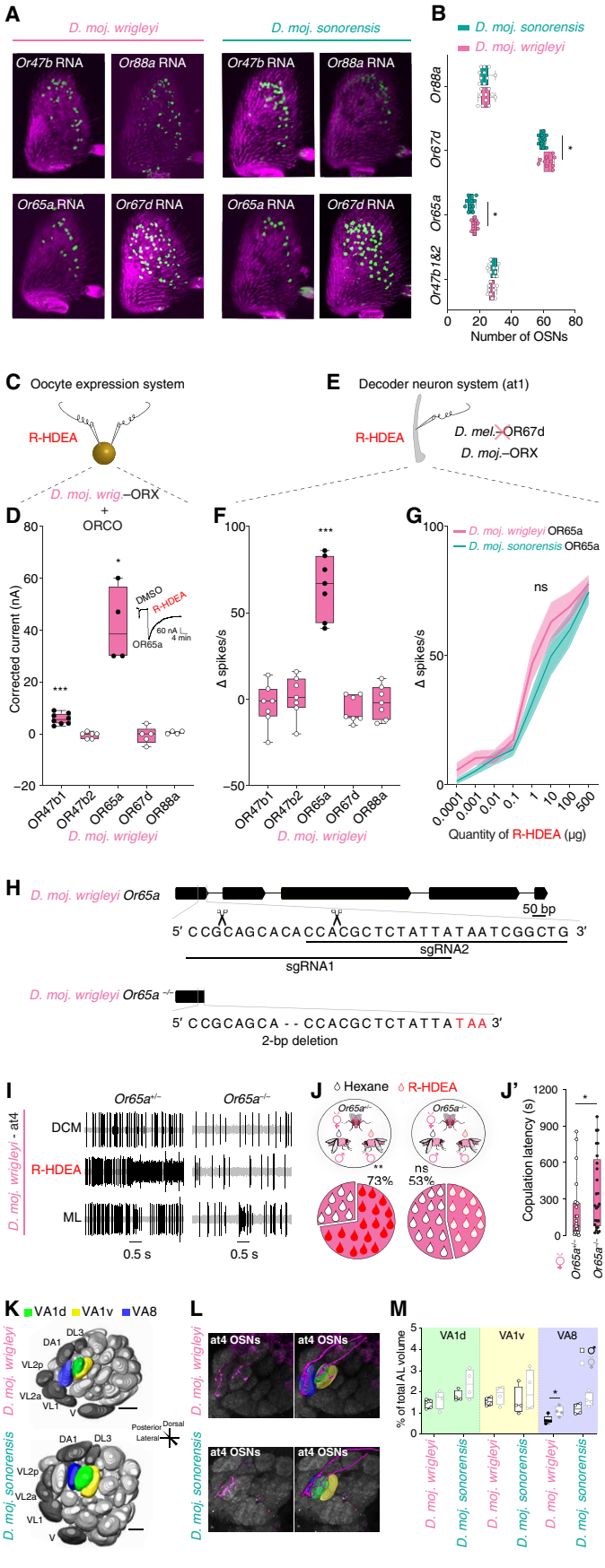

Fig. 5. Conserved peripheral sensory pathways for R-HDEA detection among *D. mojavensis* subspecies. (**A**) Expression of olfactory receptor genes (*OrX*: *Or47b*, *Or88a*, *Or65a*, and *Or67d*) in *D. moj. wrigleyi and D. moj. sonorensis* female antennae. See Materials and Methods and fig. S5A for the receptor terminology. Because of the high degree of sequence identity (99.1%) of the *Or47b*-related loci (data file S1), cross-hybridization between probes and mRNAs is likely to occur. (**B**) Number of the *Or*-expressing cells (*OrX*: *Or47b*, *Or88a*, *Or65a*, and *Or67d*) in *D. moj. wrigleyi* and *D. moj. sonorensis* females. Filled circles indicate significant differences between species. Mann Whitney *U* test; ns, $P > 0.05$; $^*P < 0.05$ ($n = 10$ antennae). (**C**) Schematic of voltage-clamp recordings from *X. laevis* oocytes ectopically expressing the different ORs (ORX) together with ORCO. (**D**) Electrophysiological responses of oocytes expressing different OR genes to R-HDEA (1 mM). In this panel and in (F), filled circles indicate significant differences from the solvent response. Mann Whitney *U* test; ns, $P > 0.05$; $^*P < 0.05$; $^{***}P < 0.001$ ($n = 4$ to 8 recordings). See fig. S5B for responses to other compounds. Right: Traces of electrophysiological responses of *D. moj. wrigleyi*–OR65a to DMSO and R-HDEA. (**E**) Schematic of ORs (ORX) expressed in *D. melanogaster* at1 neurons. (**F**) Electrophysiological responses of five ORs expressed in *D. melanogaster* at1 neurons to R-HDEA (10 μg). Mann Whitney *U* test; ns, $P > 0.05$; $^{***}P < 0.001$ ($n = 7$ recordings). See fig. S5C for responses to other compounds. (**G**) Electrophysiological responses of *D. moj. wrigleyi* or *D. moj. sonorensis* OR65a toward increasing concentrations of R-HDEA ($n = 8$ recordings). Two-way ANOVA followed by Sidak's multiple comparison test between the two subspecies' responses to the same stimulus; ns, $P > 0.05$. (**H**) Schematics of the *D. moj. Or65a* locus illustrating the single guide RNA (sgRNA) binding sites. Scissors denote the presumed cutting site. The *Or65a* loss-of-function allele carries a 2–base pair (bp) deletion in exon 1, resulting in a premature stop codon (highlighted in red). See fig. S5 (E and F) for details on generating *white* gene knockouts using CRISPR-Cas9. (**I**) Electrophysiological responses of *Or65a* heterozygous (left) and homozygous (right) animals to hexane, R-HDEA, and methyl laurate [ML; diagnostic odor for OR47b and OR88a (*13*)]. The responses to ML show an intact neuronal excitation of the Or65a-neighboring neuron(s). See fig. S5D regarding quantification of SSR responses. (**J**) Competition between two males of *D. moj. wrigleyi*, perfumed with R-HDEA (red droplet) or hexane (black droplet), to copulate with a transgenic virgin female of the same subspecies. Left: Heterozygous animal at the *Or65a* locus ($n = 148$); right: homozygous mutant at the *Or65a* locus ($n = 128$). Filled droplets indicate a significant difference between the rival males. χ^2 test; ns, $P > 0.05$; $^{**}P < 0.01$. All males and females used in this and other panels were 10-day-old virgin flies. (**J′**) Copulation latencies in seconds for *Or65a* heterozygous (left) and homozygous (right) females courted by wild-type males (single-pair assays). Filled circles indicate significant differences between both transgenic females. Mann Whitney *U* test; ns, $P > 0.05$; $^*P < 0.05$ ($n = 25$). (**K**) Three-dimensional reconstruction of antennal lobes from representative female brains of *D. moj. wrigleyi* and *D. moj. sonorensis*. Neurobiotin-marked neurons in (L) are highlighted: VA1d (green), VA1v (yellow), and VA8 (blue, only present in *D. moj. wrigleyi* and *D. moj. sonorensis*). Landmark glomeruli (dark gray, DA1, DL3, VL2p, VL2a, VL1, and V glomeruli) are used to support the homology of these three glomeruli in both *D. mojavensis* subspecies. VA8 is located ventrally to VA1v and anterior to VL2a in an area far off the DL3 glomerulus, which is targeted by Or65a neurons *in D. melanogaster*. See fig. S6A for details on the glomeruli' volumes in both subspecies. Scale bars, 20 μm. (**L**) Left top: Fluorescence staining for neurobiotin (magenta) and nc82 (gray) of *D. moj. wrigleyi* antennal lobe, backfilled from the at4 sensillum in *D. moj. wrigleyi* (identified by electrophysiological recordings; Fig. 4E). Right top: Reconstruction of the neurobiotin-marked neurons and their corresponding glomeruli reveals at4-housed neurons project to three glomeruli (*D. mojavensis* VA8, VA1v, and VA1d). Left bottom: Neurobiotin-backfilled neurons from at4 sensillum in *D. moj. sonorensis* that innervate similar regions in antennal lobe. Images in the four panels correspond to a projection of 40 Z-stacks (watch movies S7 and S8). Right bottom: Landmark glomeruli were labeled according to their positions based on the map of the *D. melanogaster* AL (*16*) (see Materials and Methods). See fig. S6B for more details. See fig. S6 (C to F) and movie S9 for backfilling of at1 sensilla. (**M**) Volumes of VA1d, VA1v, and VA8 glomeruli normalized to the total antennal lobe volume in *D. moj. wrigleyi* and *D. moj. sonorensis* (males, black; females, gray). Filled circles indicate significant difference between sexes of the same subspecies. Mann Whitney *U* test; ns, $P > 0.05$; $^*P < 0.05$ ($n = 4$ to 6 brains).

the only sexually dimorphic unit, being 1.6-fold larger in females (Fig. 5M and fig. S6, G and H). In addition, there was a nonsignificant trend of larger volume of VA8 in *D. moj. sonorensis* females compared with males (Fig. 5M and fig. S6, G and H). Together, these results indicate that OR65a-expressing neurons in both subspecies detect R-HDEA and exhibit similar innervation pattern in the antennal lobe.

Subspecies-specific contributions of R-HDEA and auditory cues in sexual isolation

As *D. moj. wrigleyi* females can distinguish between their con-subspecific males and *D. moj. sonorensis* males [which lack R-HDEA (Fig. 2, A and B); Figs. 1C and 6A], we asked whether R-HDEA mediates this discrimination. We presented to a *D. moj. wrigleyi* female a choice of a *D. moj. wrigleyi* male perfumed with hexane and a male of *D. moj. sonorensis* perfumed with R-HDEA. Female preference for its con-subspecific male was greatly reduced (Fig. 6A′ and fig. S7A). Furthermore, when given a choice between two males of *D. moj. sonorensis*, of which only one was perfumed with R-HDEA, *D. moj. wrigleyi* females exhibited a strong preference for the perfumed ones (Fig. 6A″).

Despite this instructive role of R-HDEA in mate discrimination, we observed that *D. moj. wrigleyi–Or65a* mutant females (which cannot detect R-HDEA) still display strong preference for con-subspecific males (Fig. 6B), indicating that other cues must exist. Previous reports revealed that subspecies-specific songs during courtship induce mate recognition among *D. mojavensis* subspecies (*34*). We therefore investigated whether auditory inputs are sufficient to mediate mate recognition. Aristaless *D. moj. wrigleyi* females—lacking an essential part of the antennal auditory organ—still exhibited normal preference for aristaless con-subspecific males over aristaless hetero-subspecific ones (Fig. 6B′). However, aristaless, *Or65a* mutant females exhibited a major loss in the recognition of con-subspecific males (Fig. 6B”). These results indicate that R-HDEA and auditory cues have redundant roles in permitting subspecies discrimination of *D. moj. wrigleyi*.

In contrast to *D. moj. wrigleyi* females, *D. moj. sonorensis* females preferred con-subspecific males over the *D. moj. wrigleyi* one, even when the con-subspecific one was perfumed with R-HDEA or other male-specific compounds (Fig. 6C and fig. S7B). This subspecies appears to rely solely on auditory input for subspecies recognition, as aristaless females displayed indiscriminate preference for con-subspecific and hetero-subspecific males (Fig. 6C’).

DISCUSSION

Modifications in sex pheromones and their cognate sensory detection mechanisms are thought to provide a rapid means to alter mate recognition abilities during the evolution of new species (*3*). Our results provide several insights into how intra- (between *D. mojavensis* subspecies) and interspecific (between species across *Drosophila* genus) sexual barriers arise.

First, among *D. mojavensis* subspecies, we identified four male-specific acetates of which three were exclusively produced by the northern subspecies (Fig. 2, A and B). This marked change in chemical profile is unexpected given the relatively short divergence time of ~0.25 million years between *D. mojavensis* subspecies (*18*, *19*). Although these subspecies use different host cacti in nature (*18*), they were bred on the same food in our study, suggesting that the

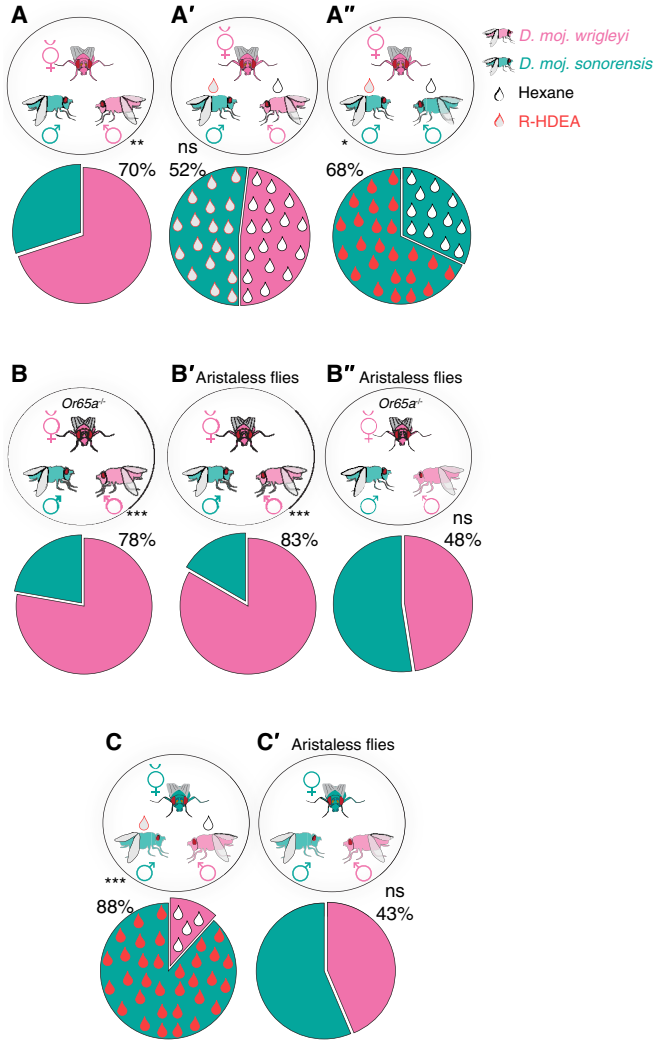

Fig. 6. R-HDEA and auditory cues collaborate to define sexual isolation among *D. mojavensis* subspecies. (**A**) Competition between two males of different subspecies to copulate with a *D. moj. wrigleyi* virgin female ($n = 80$). Pie charts in (A) to (C′) represent copulation success (%) of the rival males. χ^2 test; ns, $P > 0.05$; $^{**}P < 0.01$; $^{***}P < 0.001$. All males and females used in this and other panels were 10-day-old virgin flies. (**A′**) Competition between two males of different subspecies, *D. moj. sonorensis* perfumed with R-HDEA (red droplet) and *D. moj. wrigleyi* perfumed with hexane (black droplets), to copulate with a *D. moj. wrigleyi* virgin female ($n = 108$). See fig. S7A for details regarding the S-HDEA– and HDA-perfumed males. (**A″**) Competition between two males of *D. moj. sonorensis*, perfumed with R-HDEA (red droplet) or hexane (black droplet), to copulate with a *D. moj. wrigleyi* virgin female ($n = 76$). (**B**) Competition between two males of different subspecies, *D. moj. sonorensis* and *D. moj. wrigleyi*, to copulate with a *D. moj. wrigleyi* virgin female that lacks the R-HDEA–detecting channel Or65a ($n = 72$). (**B′**) Competition between two aristaless males of different subspecies, *D. moj. sonorensis* and *D. moj. wrigleyi*, to copulate with an aristaless *D. moj. wrigleyi* virgin female ($n = 48$). (**B″**) Competition between two aristaless males of different subspecies, *D. moj. sonorensis* and *D. moj. wrigleyi*, to copulate with an aristaless *D. moj. wrigleyi* virgin female that lacks the R-HDEA–detecting channel Or65a ($n = 84$). (**C**) Competition between two males of different subspecies, *D. moj. sonorensis* perfumed with R-HDEA (red droplet) and *D. moj. wrigleyi* perfumed with hexane (black droplets), to copulate with a *D. moj. sonorensis* virgin female ($n = 68$). See fig. S7B for details regarding the S-HDEA– and HDA-perfumed males. (**C′**) Competition between two aristaless males of different subspecies, *D. moj. sonorensis* and *D. moj. wrigleyi*, to copulate with an aristaless *D. moj. sonorensis* virgin female ($n = 64$).

different chemical profiles are not a consequence of nutrition but rather genetically determined. The male-specificity and copulation-dependent transfer of these acetates resembles *c*VA in *D. melanogaster*, which is produced by the ejaculatory bulb and transferred to females during mating. Our data reveal, however, that the sex-specific *c*VA-induced behaviors in *D. melanogaster* (*12*, *28*), inhibiting male and inducing female mating behaviors, are mediated by different compounds in *D. mojavensis*. OCDA is present and suppresses male courtship in both *D. mojavensis* subspecies, while R-HDEA induces female receptivity in the subspecies that produce it. Consistent with OCDA-induced behaviors, a recent study (*35*) showed that *D. mojavensis* males avoid courting females perfumed with ejaculatory bulb extracts of mature males.

Second, our results address a long-standing mystery of the modalities that determine prezygotic isolation between *D. mojavensis* subspecies (*25*, *26*). *D. mojavensis* subspecies display identical courtship elements, indicating that the sexual isolation (Fig. 1C) is due to different subspecies-specific traits and preferences. We provide evidence that the dedicated R-HDEA–sensing neurons and auditory cues collaborate to mediate mate recognition in *D. moj. wrigleyi*. By contrast, R-HDEA did not induce any behavioral change in *D. moj. sonorensis* females that rely only on auditory cues [i.e., the subspecies-specific song (*34*)] for mate recognition. The notable change of R-HDEA–induced behaviors (Fig. 4C and fig. S4D)—despite its conserved peripheral sensory pathway (Figs. 5E and 6, B and C)—implies the existence of differences in the central processing pathways among *D. mojavensis* subspecies. These findings are reminiscent of sexually dimorphic behavioral responses to *c*VA in *D. melanogaster* (*36*), which are thought to arise from sex-specific central neuronal connectivity patterns downstream of nondimorphic sensory neuron populations (*37*).

Third, although males of *D. melanogaster* and some Hawaiian *Drosophila* species have been shown to attract females over distance by releasing pheromones in fecal droplets (*38*, *39*), the release of droplets during close courtship has not, to our knowledge, been described in other drosophilid species. In *D. moj. wrigleyi*, this droplet contains the volatile sex pheromone R-HDEA (fig. S2G), which increases female receptivity. Such a trait might be related to the sexual behavior of *D. mojavensis* observed in nature, where males attract females to undamaged areas next to the necrotic feeding sites on cacti (*38*).

Fourth, the presence of different male-specific compounds in *D. mojavensis* compared with other drosophilids (*9*)) raises the possibility of a rapid divergence in the tuning of the corresponding sensory receptors (*23*, *31*). We demonstrate that the diverged OR65a orthologs of *D. mojavensis* and *D. melanogaster* (fig. S4J) have different functional properties; the *D. melanogaster*–Or65a is not detecting the best ligand of *D. moj. wrigleyi*–OR65a, R-HDEA, and vice versa (Fig. 4E and figs. S4I and S5C). In line with the functional divergence, the number of Or65 gene copies is frequently changing along the *Drosophila* phylogeny (*11*), indicating that the variation at this locus could be important for the evolution of novel olfactory channels (*11*).

Last, divergence of the chemosensory genes among closely related *Drosophila* species could be accompanied by a physiological alteration in the underlying central circuitry (*8*). Our results provide, to our knowledge, the first correlation between anatomical difference and divergent behaviors of homologous neurons. The likely conserved innervation pattern of neurons expressing *Or47b* and *Or88a* implies that Or65a neurons in *D. melanogaster* and *D. mojavensis* have evolved novel projection patterns in the antennal lobe, targeting DL3 in *D. melanogaster* and VA8 in *D. mojavensis*. The intriguing wiring of the Or65a in *D. mojavensis* indicates that it could be partnering with another subset of second-order neurons responsible for the different type of sexual behaviors: Or65a mediates female receptivity in *D. moj. wrigleyi*, whereas it inhibits female attraction toward *c*VA in *D. melanogaster* (*40*). However, more advanced genetic tools will be necessary to confirm this anatomical difference and to functionally characterize the olfactory pathways of the *D. mojavensis* subspecies.

Future evolutionary investigations of the innervation pattern of R-HDEA–responsive neurons in the higher brain centers will shed light on the divergent functions of R-HDEA among the closely related subspecies of *D. mojavensis* and will explain how neural circuits coevolve with sex pheromones to permit specific mate recognition.

MATERIALS AND METHODS

Drosophila lines and chemicals

Fly stocks

Wild-type flies used in this study were obtained from the National *Drosophila* Species Stock Centre (http://blogs.cornell.edu/drosophila/). Stock numbers and breeding diets are listed in table S1. Transgenic *D. melanogaster* flies and *D. mojavensis* knockout lines generated in this study are listed in table S1. All flies were reared at 25°C, 12-hour light:12-hour dark, and 50% relative humidity. For more details on the food recipes, see the *Drosophila* Species Stock Centre (http://blogs.cornell.edu/drosophila/recipes/) or (*41*).

Chemicals

Odorants used in this study, sources, and Chemical Abstracts Service (CAS) numbers are listed in the table S1. All odors were diluted in dichloromethane (DCM) for SSR, in dimethyl sulfoxide (DMSO) for oocytes and tip recording experiments, or in hexane for behavioral experiments.

Chemical analyses

Thermal desorption–GC-MS

Individual flies or ejaculatory bulbs were prepared or dissected, respectively, for chemical profile collection as described previously (*13*), with some modifications. Briefly, the GC-MS device (Agilent GC 7890A fitted with an MS 5975C inert XL MSD unit; www.agilent.com) was equipped with an HP5-MS UI column (19091S-433UI; Agilent Technologies). After desorption at 250°C for 3 min, the volatiles were trapped at −50°C using liquid nitrogen for cooling. To transfer the components to the GC column, the vaporizer injector was heated gradually to 270°C (12°C/s) and held for 5 min. The temperature of the GC oven was held at 50°C for 3 min, gradually increased (15°C/min) to 250°C and held for 3 min, and then to 280°C (20°C/min) and held for 30 min. For MS, the transfer line, source, and quad were held at 260°, 230°, and 150°C, respectively. Eluted compounds for this and the following analyses were ionized in electron ionization source using electron beam operating at 70-eV energy, and their mass spectra were recorded in positive ion mode in the range from mass/charge ratio (*m*/*z*) 33 to 500. Anal droplets of courting males were collected on a glass coverslip (22 × 22 mm, catalog no. 631-0126; https://uk.vwr.com) and analyzed by thermal desorption–GC-MS (TD-GC-MS). The structures of the identified acetates were confirmed by comparing their mass spectrum with synthesized standards.

Body extract analysis by GC-MS

Fly body extracts were obtained by washing single flies of the respective sex, age, and mating status in 10 μl of hexane for 30 min. For GC stimulation, 1 μl of the odor sample was injected in a DB5 column (Agilent Technologies; www.agilent.com), fitted in an Agilent 6890 gas chromatograph, and operated as described previously (*42*). The inlet temperature was set to 250°C. The temperature of the GC oven was held at 50°C for 2 min, increased gradually (15°C/min) to 250°C, which was held for 3 min, and then to 280°C (20°C/min) and held for 30 min. The MS transfer line, source, and quad were held at 280°, 230°, and 150°C, respectively. Average amounts of HDEA, HDA, and OCDA from individual flies were quantified by comparing their peak areas with the area of hexadecane (10 ng), which was added to the fly extract as an internal standard.

Chiral chromatography

To check the ratio of (2*R*,10*Z*)-10-heptadecen-2-yl acetate and (2*S*,10*Z*)-10-heptadecen-2-yl acetate (R/S-HDEA), hexane body extracts of male flies were injected into a CycloSil B column (112-6632, Agilent Technologies; www.agilent.com) fitted in an Agilent 6890 gas chromatograph and operated as follows: The temperature of the GC oven was held at 40°C for 2 min and then increased gradually (10°C/min) to 170°C, then to 200°C (1°C/min), and, last, to 230°C (15°C/min), which was held for 3 min.

Matrix-assisted laser desorption/ionization–time-of-flight

MALDI-TOF experiments of 13-day-old flies were performed on MALDI Micro MX (Waters, UK) operated in a reflectron mode with acceleration and plate voltages at 12 and 5 kV, respectively. Because of the relative high volatility and weaker ionization of R/S-HDEA and HDA compared with OCDA, only OCDA signals were detected in the mass spectrometry imaging (MSI) spectra. Moreover, OCDA was predominantly present in a form of $[M + K]^+$ adducts. Delayed extraction time was 500 ns. The compound's desorption/ionization was realized by nitrogen ultraviolet (UV) laser (337 nm, 4-ns pulse of maximum 320 μJ, and frequency of 20 Hz). Matrix ions were suppressed with a low mass cutoff set at *m/z* 150. Flies were fixed on their dorsal side and processed as described previously (*43*). The number of laser shots per spot was optimized and set to 60 (128 μJ per shot). The range of the measured masses was set from *m/z* 100 to 1000. Data were collected with MassLynx 4.0 software and processed with custom-made software MALDI Image Convertor (Waters, UK) to obtain spatially differentiated data. These data were exported to the BioMap software (Novartis, Switzerland) and converted to two-dimensional ion intensity heat maps. All samples were analyzed in positive ion mode and imaged using a step size of 100 μm. Methanolic solution of lithium 2,5-dihydroxybenzoate (LiDHB) and lithium vanillate (LiVA) (in case of copulated flies) matrix in a concentration of 20 mg/ml was sprayed on the fly samples by an airbrush. For one sample, 0.4 ml of LiDHB/LiVA matrix solution was used to form approximately 25 layers. Waiting time between two consecutive sprays was 3 s. LiDHB and LiVA matrices were synthesized, as described previously (*44*). Polyethylene glycol oligomers (with average molecular weights of 200, 300, 600, and 1000 Da) for calibration of the mass spectrometer were purchased from Sigma-Aldrich, as well as precursors of the LiDHB and LiVA. Potassiated adducts of OCDA at *m/z* 487 evinced a negative mass shift, which was observed within a range from *m/z* 0.05 to 0.3 between measurements.

Fly odor analysis by solid-phase microextraction

Volatiles were collected from 20 *D. moj. wrigleyi* males trapped in a mesh inside capped 4-ml glass vials with polytetrafluoroethylene-lined silicone septa (Sigma-Aldrich, 23242-U) to preclude flies' contact to the solid-phase microextraction (SPME) fiber (gray hub plain; coated with 50/30-μm divinylbenzene/carboxen on polydimethylsiloxane on a StableFlex fiber, Sigma-Aldrich, 57328-U). SPME fiber was exposed to the trapped flies for 1 hour at room temperature. The SPME fiber was then retracted and immediately inserted into the GC-MS system (Agilent 7890B fitted with MS 5977A unit) as operated previously (*45*). The inlet temperature was set to 250°C. The temperature of the GC oven was held at 40°C for 3 min and then increased gradually (5°C/min) to 280°C, which was held for 10 min.

Perfuming flies with hexane or male-specific compounds

Male and female flies were perfumed with the acetates singly diluted in hexane or hexane alone as previously described (*13*). Briefly, 10 μl of a stock solution (50 ng/μl) was pipetted into a 1.5-ml glass vial. After evaporating the hexane under nitrogen gas flow, 10 flies were transferred to the vial and subjected to three medium vortex pulses lasting for 30 s, with a 30-s pause between each pulse. Flies were transferred to fresh food to recover for 2 hours and then introduced to the courtship arenas or subjected to GC-MS analysis to confirm the increased amount of the perfumed acetate. Each fly was coated with ~1 to 3 ng of the compound of interest. This amount is comparable to that naturally present on male flies (Fig. 2C).

Chemical identification and synthesis

Provided in Supplementary Materials text S1.

Behavioral experiments

Single and competitive mating assays

Males and females were collected after eclosion and raised individually and in groups, respectively. For each experiment, courtship assays were performed in a chamber (1-cm diameter by 0.5-cm depth) covered with a plastic slide. Courtship behaviors were recorded for 10 or 20 min using a GoPro Camera 4 or Logitech C615 as stated in the figure legends. All single mating experiments were performed under red light (660-nm wavelength) at 25°C and 70% humidity. Each video was analyzed manually for copulation success, which was measured by the percentage of males that copulated successfully, copulation latency, which was measured as the time taken by each male until the onset of copulation, and courtship index, which was calculated as the percentage of time that the male spends courting the female during 10 min. In all competition experiments, copulation success was manually monitored for 1 hour. Freeze-killed females were used in the courtship assays to disentangle male sexual behaviors from female acceptance. Freshly mated females have been mated for the first time and were used in the experiments of Fig. 3 to ensure that the compounds transferred to females were still present.

In the competition mating assays, rival flies were marked by UV-fluorescent powder of different colors (red, UVXPBR; yellow, UVXPBB; and green, UVXPBY; purchased from Maxmax.com; https://maxmax.com/) 24 hours before the experiments. Competition assays were manually observed for 1 hour, and copulation success was scored to identify the successful rival under UV light. Females killed by freezing were used to calculate the courtship index of males in the presence of the different acetates- and hexane-perfumed females or con-specific and hetero-subspecific females. Data from competition experiments represent either females courted by both rival males or males courted with both rival females to ensure that females or males chose between rival pairs and did not simply copulate or court with the first partner they encountered. Results from

females that were only courted by one male, or males that only courted one female were excluded. For tarsi- or aristaless flies, either the first three segments of male tarsi or both aristae were clipped with a clean razor blade, and flies were kept to recover for 2 days on fresh food before introduction into the courtship arena. All courtship and copulation data were acquired by a researcher blinded to the treatment. For collecting male anal droplets, a virgin male and a decapitated female were kept in a courtship chamber covered with a glass coverslip. Males were allowed to court and discharge the anal droplets on the glass coverslips, which were then cracked to small pieces and inserted into the TD-GC-MS tubes for analysis. As a control, glass coverslips were sampled from courtship arenas containing only males.

Electrophysiological and molecular biology experiments

Single sensillum recording

Adult flies were immobilized in pipette tips, and the third antennal segment was placed in a stable position onto a glass coverslip (*46*). Sensilla types were localized under a microscope (BX51WI; Olympus) at ×100 magnification and identified by diagnostic odors stated in table S1. The extracellular signals originating from the OSNs were measured by inserting a tungsten wire electrode in the base of a sensillum and a reference electrode into the eye. Signals were amplified (Syntech Universal AC/DC Probe; Syntech), sampled (10,667.0 samples/s), and filtered (300 to 3000 Hz with 50/60-Hz suppression) via USB-Universal Serial Bus-Intelligent Data Acquisition Controller (IDAC) connection to a computer (Syntech). Action potentials were extracted using AutoSpike software, version 3.7 (Syntech). Synthetic compounds were diluted in DCM (Sigma-Aldrich, Steinheim, Germany). Before each experiment, 10 µl of diluted odor was freshly loaded onto a small piece of filter paper (1 cm^2, Whatman, Dassel, Germany) and placed inside a glass Pasteur pipette. The odorant was delivered by placing the tip of the pipette 2 cm away from the antennae. Neuron activities were recorded for 10 s, starting 2 s before a stimulation period of 0.5 s. Responses from individual neurons were calculated as the increase (or decrease) in the action potential frequency (spikes per second) relative to the prestimulus frequency. Traces were processed by sorting spike amplitudes in AutoSpike, analysis in Excel, and illustration in Adobe Illustrator CS (Adobe systems, San Jose, CA).

Tip recording

Tip recordings from tarsal sensilla were performed, as described previously (*47*). Male flies (8 to 10 days old) were immobilized in pipette tips, and the foreleg was fixed with a Scotch tape onto a glass coverslip. A reference glass electrode filled with Ringer's solution (140 mM NaCl, 3 mM $MgCl_2$, 2 mM $CaCl_2$, 10 mM D-glucose, and 10 mM Hepes, pH 7.4) was inserted into the thorax of the fly. The different tarsal sensilla were stimulated by placing a glass capillary filled with OCDA (10 µg) dissolved in DMSO on the sensillum tip. The recording electrode was connected to a preamplifier (TastePROBE, Syntech, Hilversum, the Netherlands), and the signals were collected and amplified (10×) by using a signal-connection interface box (Syntech) in conjunction with a 100- to 3000-Hz band-pass filter. Action potential measurements were acquired with a 9.6-kHz sampling rate and analyzed with AutoSpike.

RNA extraction and complementary DNA synthesis

Total RNA from single flies of *D. mojavensis* subspecies and from ~100 antennae was extracted using an RNA isolation kit (Direct-zol RNA MiniPrep, Zymo Research). First-strand complementary DNA (cDNA) was generated from 1.0 µg of total RNA, using oligo-dT_{20} primers and SuperScript III (Thermo Fisher Scientific). Derived cDNAs were used to amplify housekeeping and olfactory receptor open reading frames via polymerase chain reaction (PCR) with MyTaq DNA Polymerases (Bioline) and primers listed in table S1. PCR amplicons were cloned into pCR4-TOPO (Invitrogen) and verified by sequencing.

Sequence alignment

Available (https://flybase.org) and obtained protein-coding sequences in this study of *Or65a* and *Or47b* were analyzed in Geneious (v11.0.5). Briefly, a multiple-sequence alignment was generated using the MAFFT (v7.309) tool with E-INS-I parameters and scoring matrix 200 partitioning around medoids (PAM)/$K = 2$ as previously described (*48*). The final tree of *Or65a* orthologs was reconstructed using a maximum likelihood approach with the general time reversible (GTR) + G + I model of nucleotide substitution and 1000 rate categories of sites in Fasttree (v2.1.5). The tree was visualized and processed in Geneious.

Functional analysis of receptor genes in Xenopus oocytes

Oocyte injections and two-electrode voltage clamp recordings were described previously (*49*). Briefly, the open reading frames of *D. moj. wrigleyi Or47b1*, *Or47b2*, *Or65a*, *Or67d*, *Or88a*, and *Orco* were amplified from *D. moj. wrigleyi* cDNA using primers (table S1), adding Bam HI (forward) and Xba I (reverse) restriction sites and a Kozak sequence (GCCACC) immediately upstream of the first ATG. The PCR products were digested with Bam HI and Xba I and subcloned into the expression vector pCS2+. Maxi preps of recombinant plasmids were linearized with Not I and transcribed to complementary RNAs (cRNAs) with mMESSAGE mMACHINE SP6 kit (Thermo Fisher Scientific, Waltham, MA, USA). *X. laevis* (purchased from Xenopus Express France, Vernassal, Haute-Loire, France) oocytes were defolliculated with collagenase (1.5 mg/ml; Sigma-Aldrich Co., St. Louis, MO, USA) in Oocyte Ringer 2 solution (82.5 mM NaCl, 2 mM KCl, 1 mM $MgCl_2$, 5 mM Hepes, pH 7.5). cRNAs of each *Or* together with *D. moj. wrigleyi Orco* cRNA (50 ng each) were coinjected into the oocytes and incubated at 18°C for 3 to 5 days before recordings. Stock solutions of the tested compounds were prepared in DMSO (Sigma-Aldrich Co., St. Louis, MO, USA) and diluted to the indicated concentrations with Ringer's buffer (96 mM NaCl, 2 mM KCl, 5 mM $MgC1_2$, 0.8 mM $CaCl_2$, 5 mM Hepes, pH 7.6). The compounds mentioned in table S1 were applied to the oocytes successively at a rate of 2 ml/min, with extensive washings by Ringer's buffer in the intervals. Whole-cell inward currents were recorded by two-electrode voltage clamp with a TEC-03BF amplifier (npi electronic GmbH, Tamm, Germany) at the holding potential of −80 mV. Data were collected and analyzed by Cellworks software (npi electronic GmbH, Tamm, Germany).

Expression of olfactory receptors in D. melanogaster at1 neurons

Transgenic lines were generated according to standard procedures as described (*50*). The open reading frames of *D. moj. wrigleyi Or47b1*, *Or47b2*, *Or65a*, *Or67d*, *Or88a*, and *D. moj. sonorensis Or65a* receptors were subcloned from the corresponding pCS2+ constructs (see above) via digestion with Bam HI (catalog no. R0136, New England Biolabs) and Xba I (catalog no. R0145, New England Biolabs) and ligated into pUASt.attb (*51*) (a gift from J. Bischof) digested with Bgl II (catalog no. R0144, New England Biolabs) and Xba I (catalog no. R0145, New England Biolabs). Homozygous *UAS-OrX* lines (with transgene insertions into chromosome II) were generated at Bestgene (https://www.thebestgene.com). An $Or67d^{GAL4}$ stock (*12*) (provided by B. J. Dickson) was individually crossed to each of the transgenic *UAS-D. moj.-OrX* flies, and homozygous lines expressing

the Or gene of interest in the decoder at1 neuron of *D. melanogaster* were established. Each *UAS*-transgenic line was confirmed by sequencing of genomic DNA prepared from the final stocks.

Generation of knockout flies

Drosophila microinjections

Transgenesis of *D. mojavensis wrigleyi* was performed in-house following standard protocols (http://gompel.org/methods). For egg-laying agar plates, a few grams of Formula 4-24 Instant *Drosophila* Medium, Blue (Carolina Biological Supply Company) soaked in water was added on the surface. Embryos were manually selected for the appropriate developmental stage prior to alignment and injection. For CRISPR-Cas9–mediated genome engineering, a mix of two single guide RNAs (sgRNAs; see table S1 for sequences) targeting the *white* locus (to easily visualize a successful genome editing event), two sgRNAs targeting the *Or65a* locus (3 μM each), and Cas9 protein (2 μM) (all Synthego; sgRNAs with 2′-*O*-methyl 3′ phosphorothioate modifications in the first and last three nucleotides) was prepared. Before injection, individual sgRNAs were mixed with Cas9 protein (1.5:1) and incubated at room temperature for 10 min. All concentrations are the final values in the injection mix.

Genotyping

Individual G_0 flies were crossed to wild-type flies and G_1 adults visually screened for white-eyed flies. Single white-eyed flies were subsequently crossed to wild-type flies and G_2 flies genotyped by PCR. Genomic DNA of a single wing of each fly was isolated using the MyTaq Extract-PCR Kit (Bioline, catalog no. BIO-21126), the sgRNA-target site was PCR amplified (see table S1 for genotyping primers), and the amplicon was Sanger sequenced. Sequencing results were compared to the reference sequence using TIDE (*52*) to deconvolute sequencing traces. G_2 flies, which displayed heterozygous loss-of-function mutations at the *Or65a* or white locus, were in-crossed and independent stocks of *Or65a* and *white* loss-of-function alleles established. White-eyed flies were not used in behavioral experiments as they might exhibit lower levels of sexual activity.

Histology and antennal lobe reconstruction

RNA in situ hybridizations

RNA in situ hybridization on whole-mount antennae was performed, as previously described (*23*). In brief, both sense and antisense digoxigenin (DIG) RNA probes were generated for each *Or* gene using a DIG-RNA labeling kit (Roche, Indianapolis, IN, USA) according to the manufacturer's instructions. See table S1 for details about the oligonucleotides' sequences. RNA probes were hydrolyzed (60 mM Na_2CO_3, 40 mM $NaHCO_3$, pH 10.2) at 60°C for 1 hour, ethanol precipitated, and stored in formamide at −80°C until use. Heads of *D. moj. wrigleyi* and *D. moj. sonorensis* females were cold fixed [4% paraformaldehyde (PFA), 0.05% Tween 20 in 1× PBS] for 1 hour and then washed three times for 10 min in PBST (1× PBS and 0.1% Tween 20). Third antennal segments were dissected into cold fix, washed three times for 10 min in PBX (1× PBS and 1% Triton X-100), and incubated for 2 hours in hybridization (Hyb) buffer [50% formamide, 5× SSC, heparin (0.05 mg/ml), and 0.1% Tween 20]. Antennae were hybridized overnight at 55°C using appropriate RNA probe(s) and the next day were washed five times for 2 hours in Hyb buffer at 55°C, with the last wash leading to overnight incubation at 55°C. A wash of 20 min in Hyb buffer at 55°C and three times 10-min wash in PBST at room temperature were subsequently performed. Antennae were incubated in 1:500 anti–DIG-POD (in PBST and 1× bovine serum albumin) for 3 hours followed by three times 10-min wash in PBST. Samples were then incubated in TSA-Plus Cyanine 5 (Cy5) according to the manufacturer's instruction (Perkin Elmer, Waltham, MA, USA) for 70 min, followed by five times 10-min washes in PBST. Samples were subsequently suspended in 80% glycerol for visualization using confocal microscopy. Confocal Z-stacks were acquired using a Nikon A1Rsi inverted confocal microscope. ORNs were counted using NIS Elements Viewer (Melville, NY, USA).

Antennal lobe reconstruction

Fly brain dissections and stainings were performed, as described previously, (*33*, *53*) with some modifications as follows: Brains were dissected in PBS and fixed in 4% PFA for 30 min at room temperature, rinsed three times for 15 min in PBS with 0.3% Triton X-100 (PT), followed by incubation with mouse monoclonal nc82 antibody (1:30, CiteAb, A1Z7V1) in 4% normal goat serum (NGS) in PT (48 hours at 4°C). Samples were washed four times for 20 min in PT, incubated overnight with Alexa Fluor 633–conjugated anti-mouse antibody (1:250, A21052, Invitrogen) in NGS-PT, and rinsed four times for 20 min in PT and mounted in Vectashield (Vector Laboratories). Images were acquired with a Zeiss 710 NLO confocal microscope using a 40× or 63× water immersion objective. Reconstruction of whole antennal lobes and of individual glomeruli (four to six antennal lobes for each sex per species) was performed manually using the segmentation software AMIRA version 5.6.0 (FEI Visualization Sciences Group). Landmark glomeruli (DA1, DL3, VL2p, VL2a, VL1, and V) were labeled according to their position based on the AL atlas of *D. melanogaster* (*16*) to compare antennal lobes of *D. mojavensis* and *D. melanogaster* as previously done for a variety of nonmelanogaster species (*54*). Glomerular volume was calculated from reconstructed glomeruli using the information on voxel size from the laser scanning microscopy scans.

OSN backfilling

Trichoid sensilla in *D. mojavensis* were identified by SSR using diagnostic odor-evoked responses to R-HDEA for at4 or *c*VA for at1. After identifying the right sensillum, the recording electrode was removed, and neurons were backfilled by placing the sensillum inside a glass capillary filled with neurobiotin (Invitrogen, 2% w/v in 0.25 M KCl). Neurobiotin was allowed to diffuse into the OSNs for 2 hours. Brain staining was performed, as described above, and neurobiotin was visualized using streptavidin conjugated to Alexa Fluor 555 (1:500, S32355, Invitrogen).

Because of its position, we name the additional glomerulus innervated by *D. mojavensis* at4 neurons VA8. VA8 is located ventrally to VA1v and anterior to VL2a in an area that is distant from the DL3 glomerulus targeted by at4 neurons in *D. melanogaster*.

Scanning electron microscopy

Antennal scans were performed, as previously described (*33*). Images of the third antennal segment were acquired at ×4.5k magnification using an LEO 1450 VP scanning electron microscope with 10-kV and 11-mm working distance (Carl Zeiss).

Phylogenetic analysis, statistics, and figure preparation

Phylogenetic analysis

The phylogenetic relationship among the four *D. mojavensis* subspecies and other *Drosophila* species was determined using the recent genomic analysis of *D. mojavensis* (*22*) and the *Drosophila virilis*, *Drosophila grimshawi*, *Drosophila willistoni*, *Drosophila pseudoobscura*, *Drosophila ananassae*, *Drosophila yakuba*, *Drosophila simulans*, and

D. melanogaster FlyBase assemblies (FB2019_04). The BUSCO application (*55*) was ran using the Diptera dataset (composed of 2799 loci), and a common set of 2177 loci was obtained between all species and 9087 genes between *D. mojavensis* subspecies and *D. melanogaster*. Individual gene alignments using MUSCLE (*56*) were then concatenated, and third-base nucleotide positions (1,778,212 sites) were extracted. This dataset was subsequently ran on FastTree (v2.1.10) (*57*) with the default CAT approximation with, 20 rate categories under a GTR + G model and 1000 bootstraps to assess the support for the phylogenetic inference. For the receptor phylogeny, a multiple-sequence alignment was generated using the MAFFT (v7.309) tool with E-INS-I parameters and scoring matrix 200 PAM/$K = 2$ (*48*). The final tree was reconstructed using a maximum likelihood approach with the GTR + G + I model of nucleotide substitution and 1000 rate categories of sites in Fasttree (v2.1.5). The tree was visualized and processed in Geneious (v11.0.5).

Statistics and figure preparation

Normality test was first assessed on datasets using a Shapiro test. Statistical analyses (see the corresponding legends of each figure) and preliminary figures were conducted using GraphPad Prism v. 8 (https://www.graphpad.com). Figures were then processed with Adobe Illustrator CS5.

SUPPLEMENTARY MATERIALS

Supplementary material for this article is available at http://advances.sciencemag.org/cgi/content/full/6/25/eaba5279/DC1

View/request a protocol for this paper from *Bio-protocol*.

REFERENCES AND NOTES

1. M. G. Ritchie, Sexual selection and speciation. *Annu. Rev. Ecol. Evol. Syst.* **38**, 79–102 (2007).
2. O. Seehausen, Y. Terai, I. S. Magalhaes, K. L. Carleton, H. D. J. Mrosso, R. Miyagi, I. van der Sluijs, M. V. Schneider, M. E. Maan, H. Tachida, H. Imai, N. Okada, Speciation through sensory drive in cichlid fish. *Nature* **455**, 620–626 (2008).
3. C. Smadja, R. K. Butlin, On the scent of speciation: The chemosensory system and its role in premating isolation. *Heredity* **102**, 77–97 (2009).
4. H. T. Spieth, Courtship behavior in *Drosophila*. *Annu. Rev. Entomol.* **19**, 385–405 (1974).
5. D. S. Manoli, M. Foss, A. Villella, B. J. Taylor, J. C. Hall, B. S. Baker, Male-specific *fruitless* specifies the neural substrates of *Drosophila* courtship behaviour. *Nature* **436**, 395–400 (2005).
6. Y. Ding, A. Berrocal, T. Morita, K. D. Longden, D. L. Stern, Natural courtship song variation caused by an intronic retroelement in an ion channel gene. *Nature* **536**, 329–332 (2016).
7. O. M. Ahmed, A. Avila-Herrera, K. M. Tun, P. H. Serpa, J. Peng, S. Parthasarathy, J.-M. Knapp, D. L. Stern, G. W. Davis, K. S. Pollard, N. M. Shah, Evolution of mechanisms that control mating in *Drosophila* males. *Cell Rep.* **27**, 2527–2536.e4 (2019).
8. L. F. Seeholzer, M. Seppo, D. L. Stern, V. Ruta, Evolution of a central neural circuit underlies *Drosophila* mate preferences. *Nature* **559**, 564–569 (2018).
9. M. R. E. Symonds, B. Wertheim, The mode of evolution of aggregation pheromones in *Drosophila* species. *J Evol. Biol.* **18**, 1253–1263 (2005).
10. T. O. Auer, R. Benton, Sexual circuitry in *Drosophila*. *Curr. Opin. Neurobiol.* **38**, 18–26 (2016).
11. S. Guo, J. Kim, Molecular evolution of *Drosophila* odorant receptor genes. *Mol. Biol. Evol.* **24**, 1198–1207 (2007).
12. A. Kurtovic, A. Widmer, B. J. Dickson, A single class of olfactory neurons mediates behavioural responses to a *Drosophila* sex pheromone. *Nature* **446**, 542–546 (2007).
13. H. K. M. Dweck, S. A. M. Ebrahim, M. Thoma, A. A. M. Mohamed, I. W. Keesey, F. Trona, S. Lavista-Llanos, A. Svatoš, S. Sachse, M. Knaden, B. S. Hansson, Pheromones mediating copulation and attraction in *Drosophila*. *Proc. Natl. Acad. Sci. U.S.A.* **112**, E2829–E2835 (2015).
14. W. Liu, X. Liang, J. Gong, Z. Yang, Y.-H. Zhang, J.-X. Zhang, Y. Rao, Social regulation of aggression by pheromonal activation of Or65a olfactory neurons in *Drosophila*. *Nat. Neurosci.* **14**, 896–902 (2011).
15. A. Ejima, B. P. C. Smith, C. Lucas, W. van der Goes van Naters, C. J. Miller, J. R. Carlson, J. D. Levine, L. C. Griffith, Generalization of courtship learning in *Drosophila* is mediated by *cis*-vaccenyl acetate. *Curr. Biol.* **17**, 599–605 (2007).
16. V. Grabe, A. Strutz, A. Baschwitz, B. S. Hansson, S. Sachse, Digital in vivo 3D atlas of the antennal lobe of *Drosophila melanogaster*. *J. Comp. Neurol.* **523**, 530–544 (2015).
17. A. Couto, M. Alenius, B. J. Dickson, Molecular, anatomical, and functional organization of the *Drosophila* olfactory system. *Curr. Biol.* **15**, 1535–1547 (2005).
18. L. M. Matzkin, Ecological genomics of host shifts in *Drosophila mojavensis*. *Adv. Exp. Med. Biol.* **781**, 233–247 (2014).
19. W. J. Etges, Evolutionary genomics of host plant adaptation: Insights from *Drosophila*. *Curr. Opin. Insect Sci.* **36**, 96–102 (2019).
20. E. Pfeiler, S. Castrezana, L. K. Reed, T. A. Markow, Genetic, ecological and morphological differences among populations of the cactophilic *Drosophila mojavensis* from southwestern USA and northwestern Mexico, with descriptions of two new subspecies. *J. Nat. Hist.* **43**, 923–938 (2009).
21. A. Ruiz, W. B. Heed, M. Wasserman, Evolution of the *mojavensis* cluster of cactophilic *Drosophila* with descriptions of two new species. *J. Hered.* **81**, 30–42 (1990).
22. C. W. Allan, L. M. Matzkin, Genomic analysis of the four ecologically distinct cactus host populations of *Drosophila mojavensis*. *BMC Genomics* **20**, 732 (2019).
23. A. Crowley-Gall, P. Date, C. Han, N. Rhodes, P. Andolfatto, J. E. Layne, S. M. Rollmann, Population differences in olfaction accompany host shift in *Drosophila mojavensis*. *Proc. Biol. Sci.* **283**, 20161562 (2016).
24. B. D. Newby, W. J. Etges, Host preference among populations of *Drosophila mojavensis* (Diptera: Drosophilidae) that use different host cacti. *J. Insect Behav.* **11**, 691–712 (1998).
25. L. L. Knowles, T. A. Markow, Sexually antagonistic coevolution of a postmating-prezygotic reproductive character in desert *Drosophila*. *Proc. Natl. Acad. Sci. U.S.A.* **98**, 8692–8696 (2001).
26. T. A. Markow, Sexual isolation among populations of *Drosophila mojavensis*. *Evolution* **45**, 1525–1529 (1991).
27. W. J. Etges, M. A. Ahrens, Premating isolation is determined by larval-rearing substrates in Cactophilic *Drosophila mojavensis*. V. Deep geographic variation in epicuticular hydrocarbons among isolated populations. *Am. Nat.* **158**, 585–598 (2001).
28. S. Zawistowski, R. C. Richmond, Inhibition of courtship and mating of *Drosophila melanogaster* by the male-produced lipid, *cis*-vaccenyl acetate. *J. Insect Physiol.* **32**, 189–192 (1986).
29. J. Y. Yew, K. Dreisewerd, H. Luftmann, J. Müthing, G. Pohlentz, E. A. Kravitz, A new male sex pheromone and novel cuticular cues for chemical communication in *Drosophila*. *Curr. Biol.* **19**, 1245–1254 (2009).
30. W. van der Goes van Naters, J. R. Carlson, Receptors and neurons for fly odors in *Drosophila*. *Curr. Biol.* **17**, 606–612 (2007).
31. L. L. Prieto-Godino, R. Rytz, S. Cruchet, B. Bargeton, L. Abuin, A. F. Silbering, V. Ruta, M. Dal Peraro, R. Benton, Evolution of acid-sensing olfactory circuits in drosophilids. *Neuron* **93**, 661–676.e6 (2017).
32. T. O. Auer, M. A. Khallaf, A. F. Silbering, G. Zappia, K. Ellis, R. Álvarez-Ocaña, J. R. Arguello, B. S. Hansson, G. S. X. E. Jefferis, S. J. C. Caron, M. Knaden, R. Benton, Olfactory receptor and circuit evolution promote host specialization. *Nature* **579**, 402–408 (2020).
33. V. Grabe, A. Baschwitz, H. K. M. Dweck, S. Lavista-Llanos, B. S. Hansson, S. Sachse, Elucidating the neuronal architecture of olfactory glomeruli in the *Drosophila* antennal lobe. *Cell Rep.* **16**, 3401–3413 (2016).
34. W. J. Etges, K. F. Over, C. C. De Oliveira, M. G. Ritchie, Inheritance of courtship song variation among geographically isolated populations of *Drosophila mojavensis*. *Anim. Behav.* **71**, 1205–1214 (2006).
35. J. S. R. Chin, S. R. Ellis, H. T. Pham, S. J. Blanksby, K. Mori, Q. L. Koh, W. J. Etges, J. Y. Yew, Sex-specific triacylglycerides are widely conserved in *Drosophila* and mediate mating behavior. *eLife* **3**, e01751 (2014).
36. J. Kohl, P. Huoviala, G. S. X. E. Jefferis, Pheromone processing in *Drosophila*. *Curr. Opin. Neurobiol.* **34**, 149–157 (2015).
37. V. Ruta, S. R. Datta, M. L. Vasconcelos, J. Freeland, L. L. Looger, R. Axel, A dimorphic pheromone circuit in *Drosophila* from sensory input to descending output. *Nature* **468**, 686–690 (2010).
38. P. M. O'Grady, T. A. Markow, Rapid morphological, behavioral, and ecological evolution in *Drosophila*: Comparisons between the endemic Hawaiian *Drosophila* and the cactophilic repleta species group. *Rapidly Evolving Genes and Genetic Systems* **1**, 176–186 (2012).
39. D. Mercier, Y. Tsuchimoto, K. Ohta, H. Kazama, Olfactory landmark-based communication in interacting *Drosophila*. *Curr. Biol.* **28**, 2624–2631.e5 (2018).
40. S. Lebreton, V. Grabe, A. B. Omondi, R. Ignell, P. G. Becher, B. S. Hansson, S. Sachse, P. Witzgall, Love makes smell blind: Mating suppresses pheromone attraction in *Drosophila* females via Or65a olfactory neurons. *Sci. Rep.* **4**, 7119 (2014).
41. I. W. Keesey, V. Grabe, L. Gruber, S. Koerte, G. F. Obiero, G. Bolton, M. A. Khallaf, G. Kunert, S. Lavista-Llanos, D. R. Valenzano, J. Rybak, B. A. Barrett, M. Knaden, B. S. Hansson, Inverse resource allocation between vision and olfaction across the genus *Drosophila*. *Nat. Commun.* **10**, 1162 (2019).

42. J. Stökl, A. Strutz, A. Dafni, A. Svatos, J. Doubsky, M. Knaden, S. Sachse, B. S. Hansson, M. C. Stensmyr, A deceptive pollination system targeting drosophilids through olfactory mimicry of yeast. *Curr. Biol.* **20**, 1846–1852 (2010).
43. F. Kaftan, V. Vrkoslav, P. Kynast, P. Kulkarni, S. Böcker, J. Cvačka, M. Knaden, A. Svatoš, Mass spectrometry imaging of surface lipids on intact *Drosophila melanogaster* flies. *J. Mass Spectrom.* **49**, 223–232 (2014).
44. P. Horká, V. Vrkoslav, R. Hanus, K. Pecková, J. Cvačka, New MALDI matrices based on lithium salts for the analysis of hydrocarbons and wax esters. *J. Mass Spectrom.* **49**, 628–638 (2014).
45. P. Date, H. K. M. Dweck, M. C. Stensmyr, J. Shann, B. S. Hansson, S. M. Rollmann, Divergence in olfactory host plant preference in *D. mojavensis* in response to cactus host use. *PLOS One* **8**, e70027 (2013).
46. S. B. Olsson, B. S. Hansson, Electroantennogram and single sensillum recording in insect antennae. *Methods Mol. Biol.* **1068**, 157–177 (2013).
47. S. J. Moon, M. Köttgen, Y. Jiao, H. Xu, C. Montell, A taste receptor required for the caffeine response in vivo. *Curr. Biol.* **16**, 1812–1817 (2006).
48. K. Katoh, D. M. Standley, MAFFT multiple sequence alignment software version 7: Improvements in performance and usability. *Mol. Biol. Evol.* **30**, 772–780 (2013).
49. D.-D. Zhang, C. Löfstedt, Functional evolution of a multigene family: Orthologous and paralogous pheromone receptor genes in the turnip moth, *Agrotis segetum*. *PLOS One* **8**, e77345 (2013).
50. F. Gonzalez, P. Witzgall, W. B. Walker III, Protocol for heterologous expression of insect odourant receptors in *Drosophila*. *Front. Ecol. Evol.* **4**, 24 (2016).
51. J. Bischof, R. K. Maeda, M. Hediger, F. Karch, K. Basler, An optimized transgenesis system for *Drosophila* using germ-line-specific φC31 integrases. *Proc. Natl. Acad. Sci. U.S.A.* **104**, 3312–3317 (2007).
52. E. K. Brinkman, T. Chen, M. Amendola, B. van Steensel, Easy quantitative assessment of genome editing by sequence trace decomposition. *Nucleic Acids Res.* **42**, e168 (2014).
53. T. Dekker, I. Ibba, K. P. Siju, M. C. Stensmyr, B. S. Hansson, Olfactory shifts parallel superspecialism for toxic fruit in *Drosophila melanogaster* sibling, *D. sechellia*. *Curr. Biol.* **16**, 101–109 (2006).
54. Y. Kondoh, K. Y. Kaneshiro, K. Kimura, D. Yamamoto, Evolution of sexual dimorphism in the olfactory brain of Hawaiian *Drosophila*. *Proc. Biol. Sci.* **270**, 1005–1013 (2003).
55. R. M. Waterhouse, M. Seppey, F. A. Simão, M. Manni, P. Ioannidis, G. Klioutchnikov, E. V. Kriventseva, E. M. Zdobnov, BUSCO applications from quality assessments to gene prediction and phylogenomics. *Mol. Biol. Evol.* **35**, 543–548 (2018).
56. R. C. Edgar, MUSCLE: Multiple sequence alignment with high accuracy and high throughput. *Nucleic Acids Res.* **32**, 1792–1797 (2004).
57. M. N. Price, P. S. Dehal, A. P. Arkin, FastTree 2 – Approximately maximum-likelihood trees for large alignments. *PLOS One* **5**, e9490 (2010).
58. N. Shimosako, D. Hadjieconomou, I. Salecker, Flybow to dissect circuit assembly in the *Drosophila* brain. *Methods Mol. Biol.* **1082**, 57–69 (2014).
59. T. A. Markow, Evolution of *Drosophila* mating systems. *Evol. Biol.* **29**, 73–106 (1996).
60. L. L. Prieto-Godino, A. F. Silbering, M. A. Khallaf, S. Cruchet, K. Bojkowska, S. Pradervand, B. S. Hansson, M. Knaden, R. Benton, Functional integration of ``undead'' neurons in the olfactory system. *Sci. Adv.* **6**, eaaz7238 (2020).

Acknowledgments: We thank R. Stieber for performing immunohistochemistry experiments, I. Alali for fly rearing and conducting the blind analyses of the courtship assay, L. Zhang for the preliminary molecular data, and J. Layne for technical help in confocal imaging. We are grateful to K. Weniger, S. Lorenz, S. Trautheim, C. Hoyer, and L. Merkel for technical support, and to J. R. Arguello, L. Prieto-Godino, W. B. Walker III, and members of the Department of Evolutionary Neuroethology, MPI-CE, in Jena, Germany, for discussions. Transgenic flies were obtained from the Bloomington *Drosophila* Stock Center (NIH P40OD018537), and wild-type flies were obtained from the San Diego *Drosophila* Species Stock Center (now The National *Drosophila* Species Stock Center, Cornell University). **Funding:** This research was supported through funding by the Max Planck Society. T.O.A. is supported by a Human Frontier Science Program Long-Term Fellowship (LT000461/2015-L). B.A. is supported by an NSF grant (IOS-1456932). D.-D.Z. and C.L. are supported by the Royal Physiographic Society of Lund and the Swedish Research Council. L.M.M.'s lab was, in part, supported by an NSF grant (IOS-1557697). Research in R.B.'s laboratory is supported by ERC Consolidator and Advanced Grants (615094 and 833548, respectively). **Author contributions:** M.A.K., H.K.M.D., B.S.H., and M.K. conceived of the project. All authors contributed to the experimental design, analysis, and interpretation of results. M.A.K. prepared all the figures. M.A.K., with the help of T.O.A., designed the genetic constructs, and T.O.A. performed the microinjections for new drosophilid mutants. S.-L.L. generated reagents for the transgenic flies. A.S. identified and J.W. synthesized the previously unknown compounds. Other experimental contributions were as follows: M.A.K. [Figs. 1 to 4, 5 (C, E to J', and L), and 6; figs. S1, S2 (A to C, F, and G), S3, S4, S5 (A and C to G), S6 (B and D to F), and S7; movies S1 to S4 and S7 to S9; and data file S1], T.O.A. (Fig. 5H), V.G. and A.D.-C. (Fig. 5, K to M; fig. S6, A to G; and movies S5 to S9), B.A. (Fig. 5, A and B), D.-D.Z. and C.L. (Fig. 5D and fig. S5B), F.K. (fig. S2, B and C), and L.M.M. (Fig. 1B and figs. S1A and S6D). M.A.K. wrote the original manuscript, and M.K., T.O.A., R.B., and B.S.H. contributed to the final manuscript. All coauthors contributed to the subsequent revisions. **Competing interests:** The authors declare that they have no competing interests. **Data and materials availability:** All relevant data supporting the findings of this study and all unique biological materials generated in this study (e.g., mutant and transgenic fly strains) are available from the corresponding authors upon request.

Submitted 11 December 2019
Accepted 7 May 2020
Published 17 June 2020
10.1126/sciadv.aba5279

Citation: M. A. Khallaf, T. O. Auer, V. Grabe, A. Depetris-Chauvin, B. Ammagarahalli, D.-D. Zhang, S. Lavista-Llanos, F. Kaftan, J. Weißflog, L. M. Matzkin, S. M. Rollmann, C. Löfstedt, A. Svatoš, H. K. M. Dweck, S. Sachse, R. Benton, B. S. Hansson, M. Knaden, Mate discrimination among subspecies through a conserved olfactory pathway. *Sci. Adv.* **6**, eaba5279 (2020).

Science Advances

Mate discrimination among subspecies through a conserved olfactory pathway

Mohammed A. Khallaf, Thomas O. Auer, Veit Grabe, Ana Depetris-Chauvin, Byrappa Ammagarahalli, Dan-Dan Zhang, Sofía Lavista-Llanos, Filip Kaftan, Jerrit Weißflog, Luciano M. Matzkin, Stephanie M. Rollmann, Christer Löfstedt, Ales Svatos, Hany K. M. Dweck, Silke Sachse, Richard Benton, Bill S. Hansson and Markus Knaden

Sci Adv **6** (25), eaba5279.
DOI: 10.1126/sciadv.aba5279